THE STRUCTURE AND ORGANIZATION OF,

AND THE RELATIONSHIP BETWEEN THE

ORGANIC MATRIX AND THE INORGANIC

CRYSTALS OF EMBRYONIC BOVINE ENAMEL

DOROTHY F. TRAVIS, Ph.D., and MELVIN J. GLIMCHER, M.D.

From the Department of Orthopedic Surgery, Harvard Medical School, and the Massachusetts General Hospital, Boston

ABSTRACT

Electron microscope and electron diffraction studies of developing embryonic bovine enamel have revealed the organization of the organic matrix and the inorganic crystals. The most recently deposited inorganic crystals located at the ameloblast-enamel junction are thin plates, approximately 1300 A long, 400 A wide, and 19 A thick. During maturation of the enamel, crystal growth occurs primarily by an increase in crystal thickness. Statistical analyses failed to show a significant change in either the width or the length of the crystals during the period of maturation studied. Even in the earliest stages of calcification, the crystals are organized within the prisms so that their long axes (c-axes) are oriented parallel to the long axes of the prisms but randomly distributed about their long axes. With maturation of the enamel, the crystals become more densely packed and more highly oriented within the prisms. The organic matrix in decalcified sections of enamel is strikingly similar in its over-all organization to that of the fully mineralized tissue. When viewed in longitudinal prism profiles, the *intra*prismatic organic matrix is composed of relatively thin dense lines, approximately 48 A wide, which are relatively parallel to each other and have their fiber axes parallel to the long axes of the prisms within which they are located. Many of these dense lines, which have the appearance of thin filaments, are organized into doublets, the individual 48 A wide filaments of the doublets being separated by approximately 120 A. When observed in oblique prism profiles, the *intra*prismatic organic matrix is likewise remarkably similar in general orientation and organization to that of the fully mineralized tissue. Moreover, the spaces between adjacent doublets or between single filaments have the appearance of compartments. These compartments, more clearly visualized in cross- or near cross-sectional prism profiles, are oval or near oval in shape. Therefore, the appearance of the intraprismatic organic matrix (in longitudinal, oblique, and cross-sectional prism profiles) indicates that it is organized into tubular sheaths which are oriented with their long axes parallel to the long axes of the prisms in which they are located, but randomly oriented about their own long axes, an orientation again remarkably "blue printing" that of the inorganic crystals. The predominant feature of the walls of the tubular sheaths, when viewed in cross- or near cross-section, is that of continuous sheets, although in many cases closely packed dot-like structures of approximately 48 A were also observed, suggesting that the wall of the sheaths consists of a series of closely packed filaments. The 48 A wide dense lines (filaments) representing the width of the sheath wall were resolved into two dense strands when viewed in longitudinal prism profiles. Each strand was 12 A wide and was separated by a less electron-dense space 17 A wide. The intraprismatic organic matrix is surrounded by a prism sheath which corresponds in mineralized sections to the electron-lucent uncalcified regions separating adjacent prisms. Structurally, the prism sheaths appear to consist of filaments arranged in basket-weave fashion.

INTRODUCTION

Although a number of electron microscope studies of enamel have dealt with cellular changes associated with mineral and matrix deposition (7, 8, 26, 33, 36–38, 41, 45, 48, 64, 65, and others), and with the growth, size, and shape of enamel crystals within the matrix (10, 34, 46, 47), few investigations have dealt with the organization and the structure of the organic matrix and its relationship to the inorganic crystals (9, 10, 45–47, 49). Since there is strong evidence to suggest that the molecular configuration, the aggregation state, and the organization of organic matrices in mineralized tissues are intimately related to the initiation of mineralization and to the ultimate orientation and organization of the crystals in the tissue (1, 2, 13–16, 19, 22, 30–32, 42–44, 46–51, 53–62), the present study was undertaken to investigate the structure and organization of, and the relationship between the organic matrix of developing bovine enamel and the inorganic crystals of apatite.

MATERIALS AND METHODS

Unerupted premolar teeth were obtained from the lower jaws of approximately 5-month old calf fetuses (15, 20), and rinsed briefly in cold buffer, 0.05 M Tris, pH 7.4. The teeth were then fixed in cold buffered 1 per cent OsO_4 at pH 7.45 (28, 35) for 2 hours, rinsed in 50 per cent alcohol and dehydrated through a graded series of ethyl alcohol. Whole teeth were then embedded in either methacrylate or Epon. The technique for methacrylate embedding was as follows. The teeth were infiltrated with 25, 50, 75, and 100 per cent methyl methacrylate under vacuum, allowed to stand in 100 per cent methyl methacrylate monomer with 1 per cent or 2 per cent catalyst (Lucidol) overnight, embedded in pre-polymerized methyl methacrylate in aluminum foil boats, and allowed to complete polymerization under ultraviolet light overnight. For Epon-embedded material, the teeth were allowed to stand overnight in equal parts of propylene oxide and Epon 812 plus nadic methyl anhydride without accelerator. They were then embedded in aluminum foil boats in Epon according to Luft (27).

The polymerized Epon and methacrylate blocks were trimmed on a band saw, glued onto Plexiglas blocks with Duco cement to facilitate mounting for sectioning. Sections 100 to 300 μ thick were obtained by using a modified Gillings-Hamco apparatus. After the sections were rinsed in warm water they were thoroughly dried. Small pieces of the sectioned tooth were then dissected with a razor blade and re-embedded and oriented in gelatin capsules. For electron microscopy, thin sections were cut with diamond knives on an LKB ultramicrotome, picked up on carbon-coated Formvar grids and examined with a Siemens Elmiskop I operated at 60 kv with or without a cold stage. The microscope was calibrated to within 1 per cent to 3 per cent of the scope magnification scale with a diffraction grating replica containing 28,800 lines per inch. Either 400 μ or 200 μ condenser II apertures were used in conjunction with 50 μ objective apertures. In order to prevent sublimation of the crystals, both the preliminary examination and the taking of micrographs were carried out by using less than a 4 μamp current and with condenser II overfocused by two to four steps up to plate magnifications of 80,000 diameters.

Selected area electron diffraction was carried out with 20 μ to 30 μ diffraction apertures with or without a cold stage on consecutive sections alternating with those used for microscopy. Electron diffraction patterns were indexed by using gold as a standard.

Demineralization of thin sections of enamel was carried out on the grids, using either the same sections previously examined for microscopy or alternate consecutive sections. In order to prevent fragmentation and disorganization of the enamel filaments, marked swelling of the prisms, and solubilization of the proteins (17, 21), the grids were floated section side down on 10 per cent buffered formalin, pH 7.45, for a 24 to 48 hour period in covered spot-plates before demineralization in 0.5 M EDTA, pH 8.0, for 24 to 48 hours. The grids were rinsed either briefly in distilled water, or for 4 hours in 0.44 M KCl, 0.01 M Tris, pH 7.95 buffer, followed by distilled water for 30 minutes. Some of the grids were stained with lead (3, 25, 29, 63), others with 1 per cent phosphotungstic acid, pH 4.5 or 7.0, or saturated uranyl acetate, pH 4.2, for 1 hour.

Measurements of the dimensions of the crystals and of the components of the organic matrix were made from photographic enlargements of at least 128,000 to 500,000 from plate magnifications of at least 38,000 to 80,000 with a Bausch and Lomb measuring magnifier graduated in 0.1 mm intervals.

RESULTS

With reference to the results reported in this study, it is well to emphasize that there is increasing evidence that maturation of dental enamel is accompanied by profound changes in the amount and composition of the organic matrix (4, 18, 20) and in the water content (4), as well as changes in crystal size, habit, and orientation (34, 46, 47). Thus, in order to study the organic matrix, the
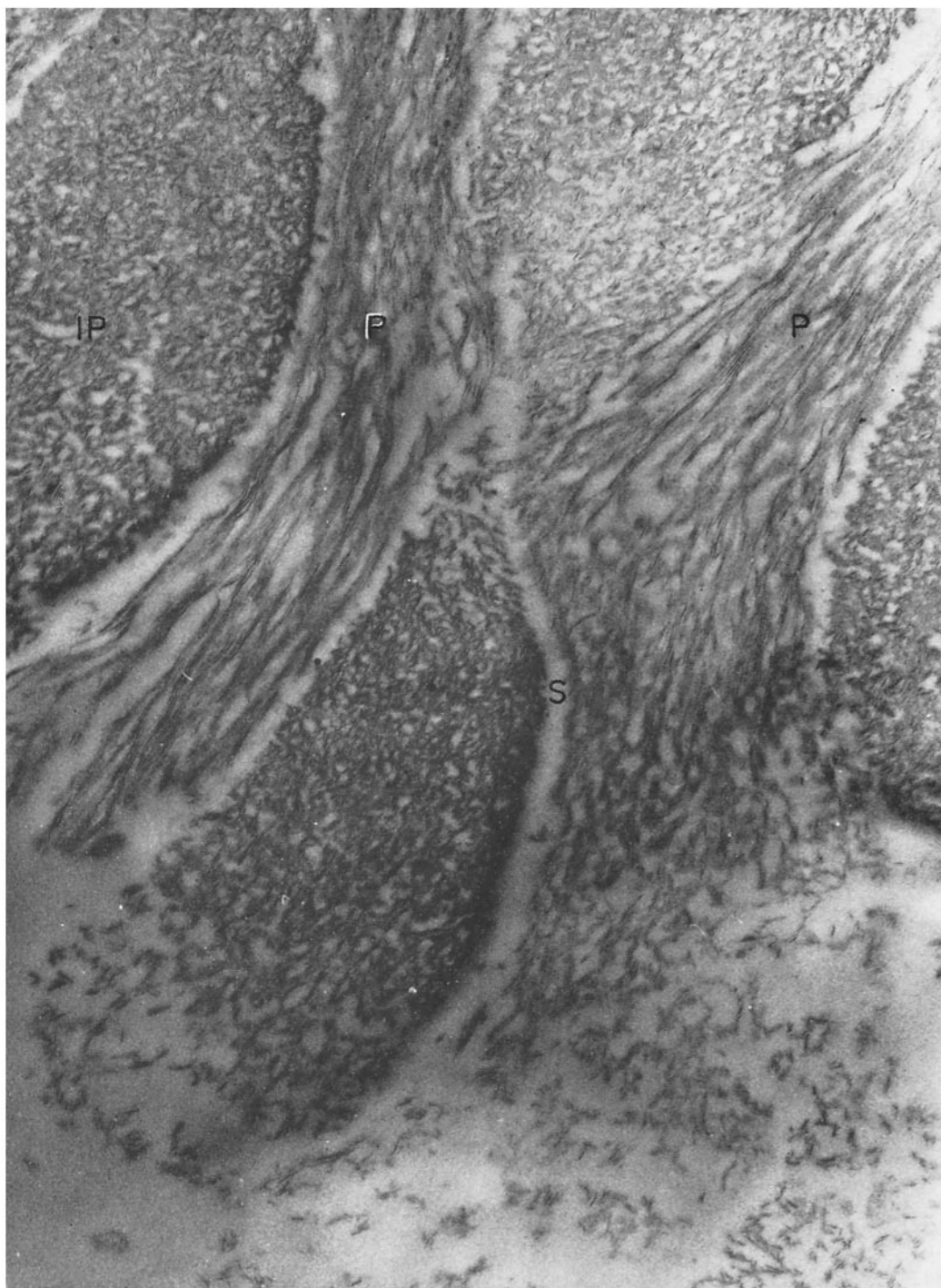
FIGURE 1 The earliest observed stage of enamel development near the AEJ. Note organization of inorganic crystals into discrete prisms in varying profiles (*P* and *IP*). The prism sheaths (*S*) are devoid of crystals and separate one prism from the next. Some polymerization damage is evident in this methacrylate section. × 32,000.

inorganic crystals, and the relationships between the two major components, it is necessary to relate the observations to the stage of enamel development. This can be done by using the age of the animal as a baseline, relating a more mature to a less developed tooth in the same embryo, or by using the same tooth of a given embryonic age and examining serially the regions from the ameloblast-enamel junction (youngest) to the enamel-dentin junction (oldest). By far the easiest and most accurate method is the latter, and this method was therefore chosen. The enamel was arbitrarily divided into three regions for this study: (a) the region near and 1 μ above the ameloblast-enamel matrix junction (AEJ); (b) the region midway between the AEJ and the enamel-dentin junction (AEJ-EDJ), approximately 30 μ from the AEJ; and (c) the region near and at the enamel-dentin junction (EDJ), approximately 60 μ from the AEJ.

Mineralized Enamel

The Ameloblast-Enamel Junction (AEJ)

In the earliest stages of enamel development observed in five-month embryonic bovine premolar teeth, the organization of the inorganic crystals into discrete prisms in varying profiles (P and IP) is already visible in Figs. 1 and 2. The prisms are surrounded by electron-lucent areas devoid of inorganic crystals, corresponding to what have been referred to as prism sheaths (S, Figs. 1, 2, 18, 32, 35). Because of the poorly defined limits of the enamel prisms at this stage of development, dimensions of prism width are more difficult to determine than in more mature regions of developing enamel. The average approximate width of the prisms lies between 1 μ and 1.5 μ when measured in cross- or oblique sections, and slightly less when measured in longitudinal sections.

The very thin electron-lucent crystal plates, arranged as tapes or ribbons (Figs. 1 to 8), show

a definite preferential orientation (Figs. 2, 3, and 5 to 8) at this early stage of prism development. In longitudinal prism profiles (Figs. 1 to 8), the crystals are oriented with their long dimensions relatively parallel to the long axis of the prism in which they are located. On the other hand, the appearance of long, broad, flat plates of low electron density and of long, thin lines of high electron density (Figs. 4 to 8), combined with the random appearance of their profiles in oblique and cross-sections (Figs. 9 and 10), indicates that the crystals are randomly oriented about their long dimensions. Selected area electron diffraction (Fig. 11 a and b) from the longitudinally oriented prisms showed marked preferential orientation of the c-axis of the crystals (00l reflections) parallel to the long axis of the prism, indicating that the long dimension of the crystals corresponds to their crystallographic c-axis.

Furthermore, the presence of the 112, 211, and 300 reflections in the electron diffraction patterns from the longitudinally oriented crystals indicates that there is little if any orientation of the crystals in a plane perpendicular to the c-axis (17). The characteristics of the selected area electron diffraction patterns (Fig. 12 a and b) from near cross- or slightly oblique sections of the prisms also indicate the random dispersion of crystals about their c-axes (17).

The average dimensions of the crystals at the AEJ region are shown in Table I. These values agree closely with those reported by Rönnholm (46) for human enamel and by Nylen et al. (34) for rat enamel.

The thinness of the crystals results in extremely low contrast when their broad faces (width) lie parallel to the plane of section, thus making it difficult to distinguish the mineral phase from the background or organic phase (Figs. 4 to 8 a). Therefore, crystal width measurements were primarily obtained from prism profiles in near or true cross-sections (Fig. 9). Crystal thickness measurements were also made from these same

FIGURE 2 A mineralized section similar to the previous one but clearly showing that the plate- or ribbon-like crystals are oriented with their long dimensions relatively parallel to the long axis of the prism (indicated by arrows) in which they are located. Note clear separation of prisms by regions free of crystals (S), and stippled material (SM) near cell surface. Epon. × 25,600.
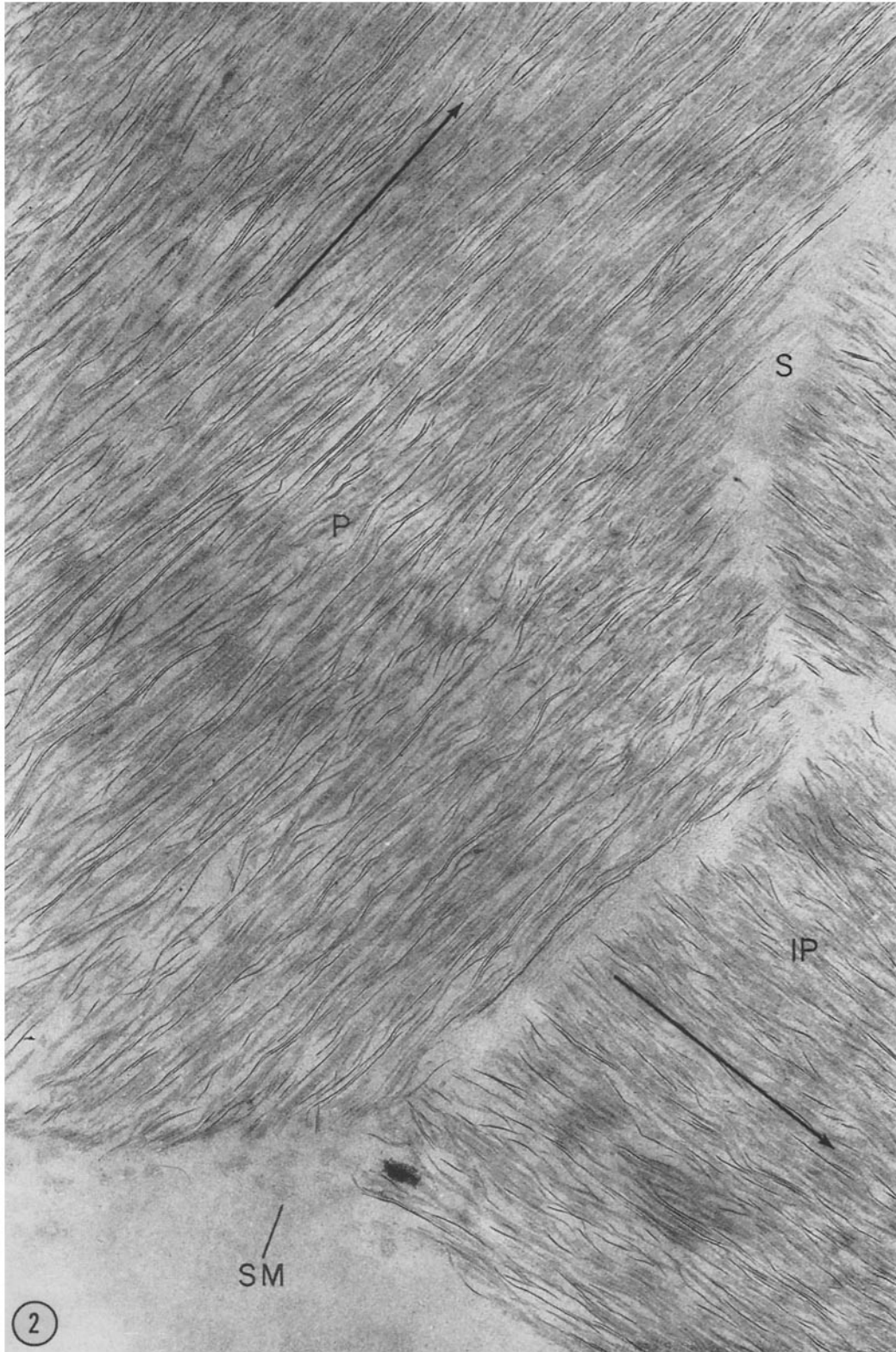
profiles, as well as from crystals viewed on edge in longitudinal sections of prisms. The lengths of the crystals were obtained from similarly dispersed crystals in longitudinal sections of the prisms. Because two or three crystals lie with their thick dimension on a line in the plane of section, they can easily be misinterpreted as a single long crystal (Figs. 4 to 8 a). Therefore, the lengths of only those crystals which showed their overlapping ends were measured (Figs. 4 to 8, arrows). The inability to clearly distinguish many of these crystals accounts for the small number measured (Table I). Another factor which contributed to the errors in length measurements and which probably accounts for the rather large standard errors observed is the fact that the crystals are not only arranged in rows in a staggered or overlapped fashion (Figs. 4, 5, 7, and 8), but on each end of the long axis of the crystal one edge appears to be tapered or longer than the other. For the foregoing reasons the order of accuracy in the measurement of crystal dimensions in any region of enamel is as follows: thickness > width > length.

Midway Between the Ameloblast-Enamel Junction and the Enamel-Dentin Junction (AEJ-EDJ)

The prism widths in this region are essentially the same as those near the AEJ. The most striking differences between this region and the AEJ region are the following (Figs. 21 to 25): (a) there is a marked improvement in the general organization and architecture of the prisms; (b) the crystals are much more electron-dense and more closely packed; (c) although the general orientation of the crystals with respect to the long axis of the prism remains unchanged, the degree of perfection of the orientation of the long dimensions (c-axes) of the crystals is improved. Despite the improvement in c-axis orientation, both electron

TABLE I

Measurements of Enamel Crystals at and near the AEJ

| Number of crystals measured	Dimension	Mean value (range)	Mean ± standard error of mean
		A	A
142	Thickness	19	19 ± 1
		(9–35)	
53	Width	381	381 ± 25
		(214–530)	
29	Length	1212	1212 ± 232
		(685–2570)	

micrographs and selected area electron diffraction patterns revealed a random rotation of the crystals about their long dimensions (c-axes) (Figs. 21 to 23, and 28 and 29).

Measurements of the crystal dimensions showed a fivefold increase in thickness over those crystals observed at the AEJ but no significant increase in either their width or length (Table II). The measurements were subject to the same errors noted previously, and an additional difficulty was introduced in this area and in the more mature EDJ region. The overlapped crystals appeared to be either separated or fractured during sectioning, as similarly noted by Nylen et al. (34). Crystal length measurements were made on the assumption that the crystals are separated rather than fractured.

In this region and in the region of the EDJ there are a number of crystals in which an electron-opaque line, approximately 19 A wide, appears to bisect the thickness dimension (Figs. 26 and 27, 37 and 38, arrows). This structure was observed in this study in very thin sections at true focus and in which no evidence of sublimation was apparent.

Figure 3   A micrograph illustrating more clearly that the young thin enamel crystals are oriented with their long dimension relatively parallel to the long axis of the prisms in which they are located. Arrows indicate long axis of prisms. Epon. × 25,600.

Figure 4   A higher magnification of young enamel crystals near the AEJ. Note the presence of stippled material (*SM*) near cell surface, the poorly defined limits of the longitudinal prism profile (*P*) and oblique prism profiles (*IP*). Also note that in the same prism (*P*) the long, broad, flat crystal plates of low electron opacity are evident with long, thin crystal profiles of higher electron opacity, indicating that the crystals are randomly oriented around their long dimensions. See also Figs. 5 to 8. Epon. × 128,000.
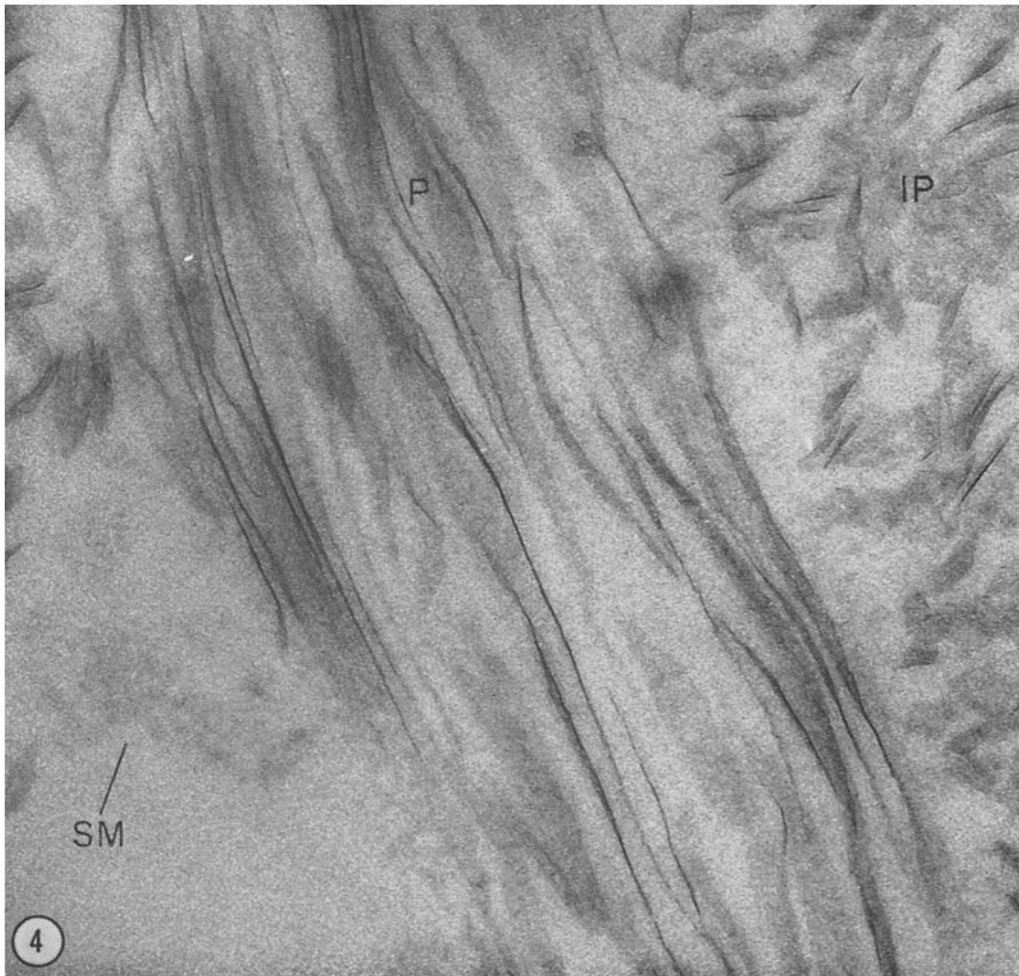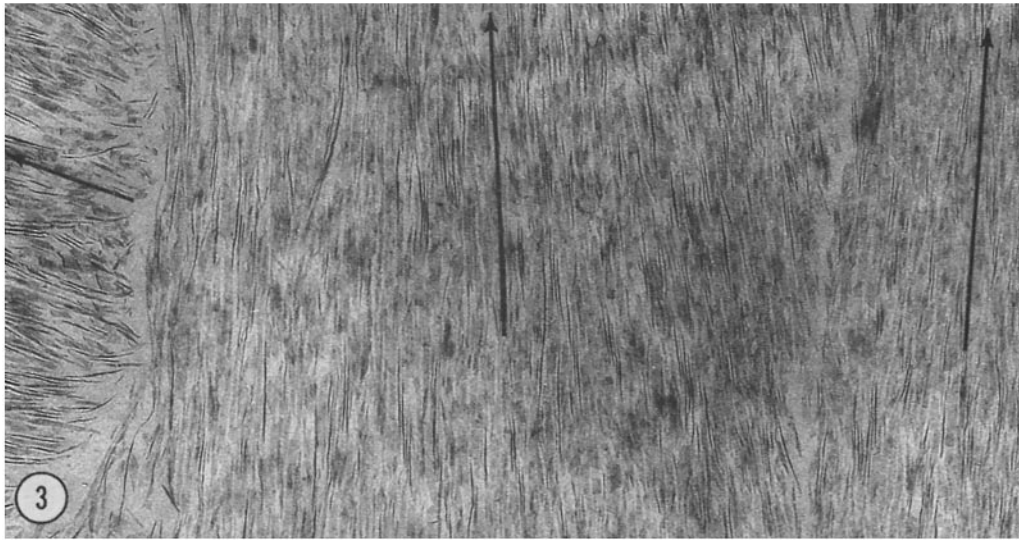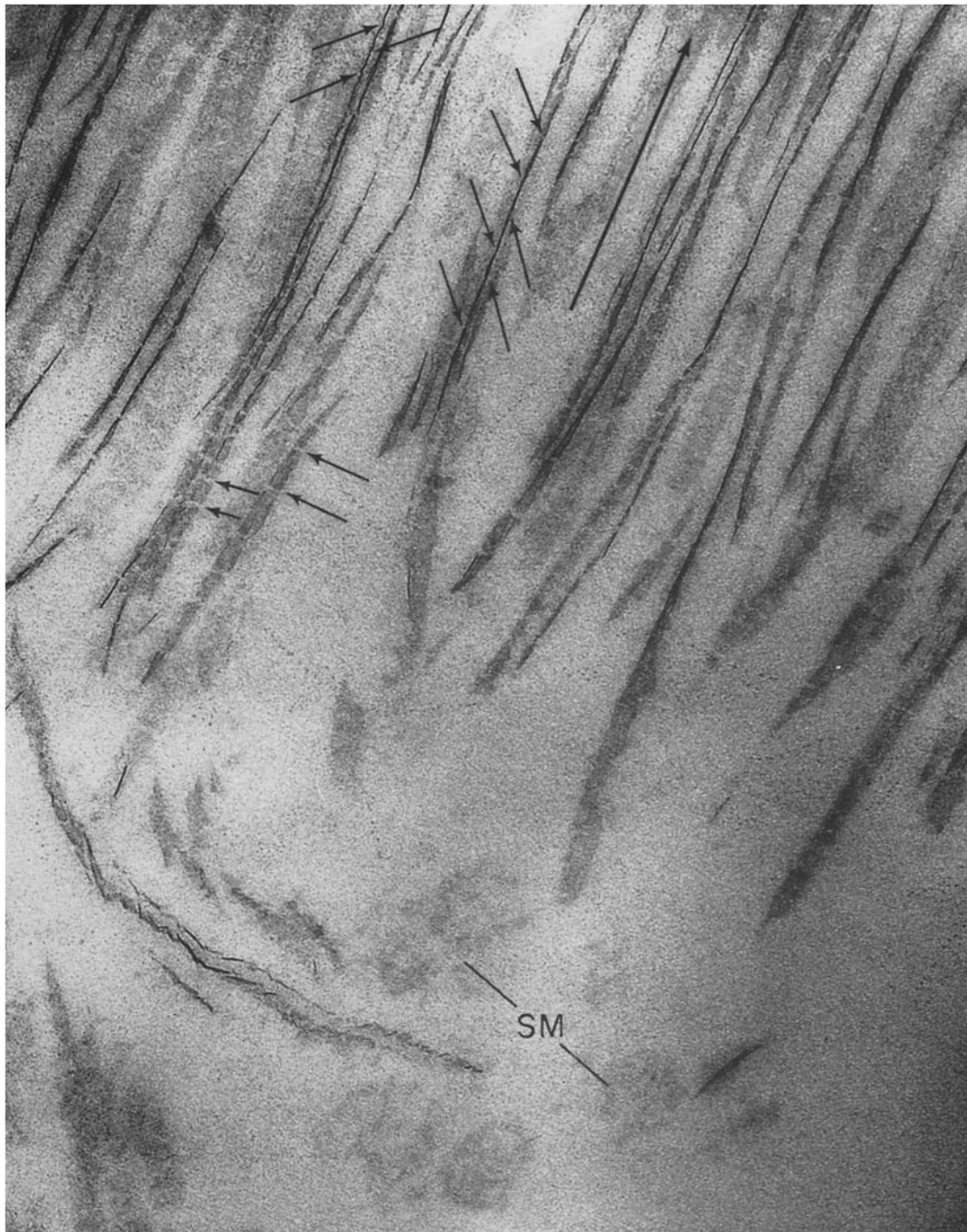
FIGURE 5 Young enamel crystals near the AEJ. Long arrow indicates direction of prism axis. Again, note that the crystals are oriented with their long axis approximately parallel to the long axis of the prism but that long, broad, flat crystal plates of low electron density are evident with long, thin crystal profiles of higher electron density, indicating that the crystals are randomly oriented around their long dimensions. Note overlaps and "gaps" of low electron density in a number of young crystals (short arrows) which lie with their thick dimensions on a line, suggesting single long crystals, also evident in Fig. 4. Similar gaps of low electron density are observed in the long, broad crystal plates. Also note stippled material (SM) near cell surface. Epon. × 128,000.

FIGURE 6 Young enamel crystals near the AEJ. The slightly underfocused micrograph fails to reveal the presence of overlaps or gaps when a number of crystals lie on edge in a single line, thus giving the impression of extremely long thin crystals. This figure serves to illustrate some of the difficulties involved in the measurement of crystal lengths. Epon. × 128,000.

FIGURE 7   Young enamel crystals near the AEJ showing that they are oriented parallel to the prism axis (indicated by long arrow) but are randomly oriented around their long dimensions. Note the overlaps observed in a number of young crystals oriented on edge (short arrows). Also note the stippled material (*SM*) near cell surface. Epon. ✕ 128,000.

THE ENAMEL-DENTIN JUNCTION (EDJ)

Few observable differences exist between the crystals near the enamel-dentin junction (EDJ) and those midway between this region and the ameloblast-enamel matrix junction (AEJ). Typical moiré patterns were frequently observed where two single crystals overlapped at varying angles. Similarly, low electron density demarcations between the long individual crystals are somewhat more clearly observed, as are the tapered edges of each end of the crystals (Figs. 37 and 38). As was stated earlier, it is these latter features which make length measurements of the crystals the least accurate of all three dimension measurements. Moreover, it is very difficult to determine whether the demarcations represent fractures of the crystals or separations of closely packed overlapping crystals. The average dimensions of the crystals are shown in Table III. The most striking change noted in the EDJ is the approximately ninefold increase in thickness of the crystals over that of crystals observed at the AEJ.

A summary of the changes in the dimensions of the crystals in the three regions of enamel studied is presented in Table IV, and an analysis of the statistically significant differences is shown in Table V. It should be emphasized that the statistical analyses must be interpreted with caution. In the first place, only a relatively small number of crystals were counted. Secondly, the difficulty of determining a true length and especially a true width of the crystals undoubtedly contributed to the variation and spread of these measurements about their mean values. The extent of the deviation about the mean value influences to a large degree the calculated probability values, so that what may appear to be (and actually may be) a slight to moderate difference in a particular dimension may not prove to be statistically significant. Therefore, a positive correlation, that is, a statistically significant change in a crystal dimension in one region as compared with another, is more meaningful than a negative one. The data in Table V clearly show that there is a highly significant increase in the thickness of the crystals in the AEJ as compared with those midway between the AEJ and EDJ, and between the crystals in the AEJ as compared with those in the EDJ. No statistically significant differences were noted in either the widths or lengths of the crystals in any one region as compared with another region. Similar findings have been reported by

TABLE II

Measurement of Enamel Crystals Midway Between the AEJ-EDJ

Number of crystals measured	Dimension	Mean value (range)	Mean ± standard error of mean
		A	A
53	Thickness	100 (45-175)	100 ± 3
24	Width	395 (300-483)	395 ± 27
24	Length	1095 (878-1405)	1095 ± 74

TABLE III

Measurement of Enamel Crystals Near the EDJ

Number of crystals measured	Dimension	Mean value (range)	Mean ± standard error of mean
		A	A
48	Thickness	167 (117-281)	167 ± 7
15	Width	554 (468-625)	554 ± 29
29	Length	1629 (704-2650)	1629 ± 142

Rönnholm (46) for developing human enamel.

Oblique and cross-sectional prism profiles terminate at approximately 12 μ from the EDJ. At this point, a region or band of well defined enamel crystals longitudinally oriented (Fig. 39) extends toward the EDJ, free of clearly defined prisms. The EDJ is characterized by an interdigitation of the enamel with the dentin (Figs. 40 and 41). The dentin is clearly defined from the enamel by its lower electron density, the presence of much smaller crystals, and the presence of the typical, $\sim$700 A, axial periods of the collagen fibrils.

Even in the interdigitations where the general organization of the prisms is lacking, the enamel crystals are still not randomly dispersed, but are so oriented that their long axes are roughly parallel to one another and to the general direction of the longitudinally dispersed crystals situated at the termination of the prisms. Selected area electron diffraction patterns again confirm that the long dimension of the crystals corresponds to their

TABLE IV

A Summary of the Changes in Crystal Dimensions in the Three Regions of Enamel Studied

| Region | Mean measurements ± standard error of mean | | |
	Thickness	Width	Length
	A	A	A
AEJ	19 ± 1	381 ± 25	1212 ± 232
Midway AEJ-EDJ	100 ± 3	395 ± 27	1095 ± 74
EDJ	167 ± 7	554 ± 29	1629 ± 142

c-axes (Fig. 42). Electron-diffraction patterns of dentin (Fig. 43) in the same section and from the same volume of tissue not only show broader reflections, but are complete rings rather than spots, confirming the visual evidence that the number of crystals per volume is considerably greater, and that, therefore, the apatite crystals in dentin are considerably smaller than those of enamel.

Demineralized Enamel: The Organic Matrix

GENERAL FEATURES AND ORGANIZATION

In undecalcified sections, irregular masses of low electron density were visualized between the surface of the ameloblasts and the inorganic crystals. This material appeared to be similar to the stippled material described by Watson (64) (Figs. 2, 4, 5, 7, and 8 *a*). After staining and partial decalcification with uranyl acetate, this material was found to be continuous with the organic matrix in which the crystals are embedded (Figs. 13 and 14). The stippled material and the organic matrix uncovered by the partial demineralization have the appearance of short, swollen, fragmented filaments (Figs. 13 and 14), probably the result of the acid-uranyl acetate treatment.

The structural subunits observed in sections of mineralized enamel were also clearly seen in sections of demineralized enamel: (*a*) prisms cut in varying profiles and containing the intraprismatic organic matrix, and (*b*) prism sheaths which surround and delineate individual prisms and which correspond to the unmineralized electron-lucent areas seen in undecalcified sections of enamel (Figs. 18, 32, 35). In decalcified sections the appearance of the enamel is strikingly similar in over-all organization to that of fully mineralized enamel (Figs. 15 to 19, 30 to 32, 35, and 49). This was true in all regions of the enamel studied.

STRUCTURAL ORGANIZATION OF THE ORGANIC MATRIX

When viewed in longitudinal prism profiles, the intraprismatic organic matrix appears to consist of relatively parallel, thin, dense lines having the appearance of filaments. The filaments are approximately 48 A wide and are arranged with their fiber axes relatively parallel to the long axes of the prisms within which they are located, similar to the orientation of the long axes of the inorganic

FIGURE 8 *a* Young enamel crystals near the AEJ. Note that the young crystals are oriented with their long axes parallel to the prism axis and that there is a random orientation of the crystals around their long axes. Also note the tape-like arrangement of the young crystals in long, broad profiles which are of low electron density, and the appearance of overlaps in rows of crystals standing on edge which are of higher electron density. The electron-dense lines across the long broad tapes similarly suggest overlaps. Stippled material (*SM*) is also seen near the cell surface. Epon. × 128,000.

FIGURE 8 *b* A high magnification showing a portion of a row of young crystals standing on edge, illustrating the overlaps (arrows) which are evident between the crystals and which, if overlooked, give the impression of extremely long crystals. Epon. × 1,007,000.
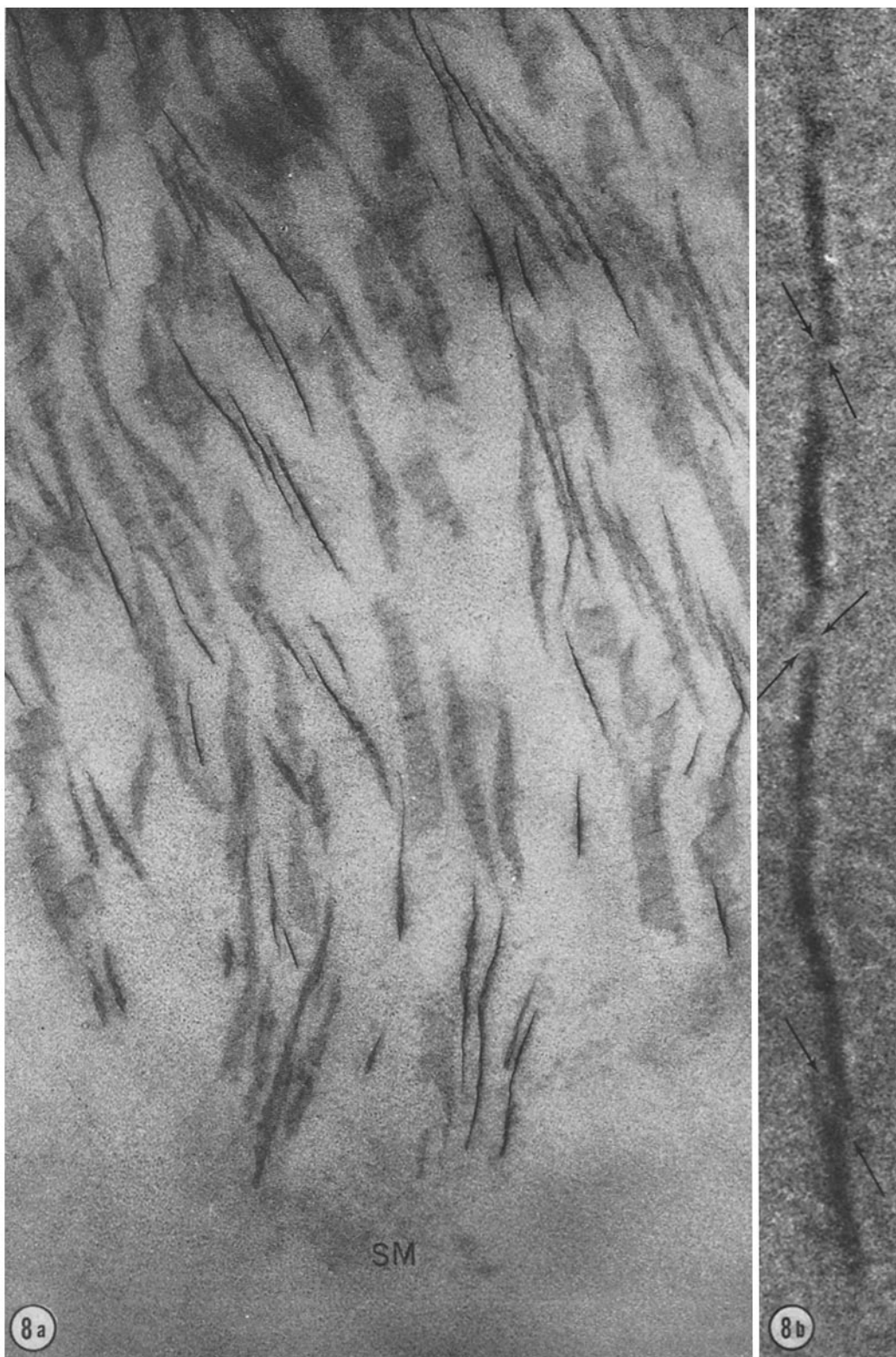
crystals (Figs. 15 to 20). Progressing from the AEJ to the region midway between the AEJ and EDJ, the intraprismatic thin filaments in longitudinal prism profile become more closely packed and more highly organized and oriented. These changes are remarkably similar to those noted in the organization and orientation of the inorganic crystals in this region as compared with the AEJ (Figs. 30 to 32). It is apparent that a number of the filaments are arranged into doublets, the individual filaments of the doublets being separated by approximately 120 A (Figs. 16, 18, 30 to 32, 44, and 45). The space between adjacent doublets or between single filaments not arranged in doublets varies a great deal. Neither the width of the individual filaments (48 A) nor the doublet space of 120 A varies significantly from the AEJ to the EDJ (Tables VI, VII, VIII, and IX), in sharp contrast with the growth in crystal thickness from the AEJ to the EDJ.

Oblique prism profiles also showed dense 48 A lines, the 120 A doublet, and the added appearance of elliptical and oval compartments between adjacent doublets or between adjacent single filaments (Fig. 18). As in the longitudinally

sectioned prisms, the over-all organization and orientation of the filaments closely parallels that of the inorganic crystals.

In cross- or near cross-sections of the prisms, the organization of the organic matrix into oval or near oval compartments is more clearly seen (Figs. 15 to 17, 30 to 32, and 36). The walls of the compartments are approximately 48 A thick, corresponding to the width of the dense lines or filaments seen in longitudinal and oblique prism profiles. Moreover, in many instances, the walls of adjacent compartments were observed to be separated by approximately 120 A, corresponding to the doublet space seen in longitudinal and oblique sections. The over-all organization of the oval compartments is random; that is, their long axes or width dimensions are randomly oriented (Fig. 36).

The size of the compartments measured in cross- or near cross-sections is shown in Table X. The rather large variations are due to the difficulty of obvious distortions of the compartments following decalcification and to the difficulties of obtaining true cross-sectional prism and compartment profiles.

In contrast with the reported occurrence of

FIGURE 9   A cross-sectional profile of a portion of a prism near the AEJ. Note the rectangular cross-sectional profiles of the crystals and that they are randomly dispersed. Methacrylate. × 124,800.

FIGURE 10   A slightly oblique section of a portion of a prism near the AEJ showing the randomly dispersed crystals. Epon. × 128,000.

FIGURES 11 and 12   Selected area electron-diffraction patterns from crystals in both longitudinal and cross-sectional prism profiles near the AEJ. Methacrylate.

Fig. 11 a. The image of the diffraction aperture over crystals in a longitudinal prism profile at the AEJ. × 18,000.

Fig. 11 b. The selected area electron-diffraction pattern from the region seen in Fig. 11 a. The arcing of the 002 and 004 reflections confirms the evidence from electron micrographs that there is a marked preferential orientation of the long c-axes of the crystals parallel to the long axis of the prism. The presence of the 112, 211, and 300 reflections indicates there is little, if any, orientation of the crystals in a plane perpendicular to the c-axis. × 2.

Fig. 12 a. The image of the diffraction aperture over crystals in a cross- or slightly oblique prism profile near the AEJ. × 18,000.

Fig. 12 b. Selected area electron-diffraction pattern of Fig. 12 a. The absence of the 00l reflections and the presence of an arced 210 oriented reflection indicates that there is some tilting of the c-axis with respect to the electron beam. The complete rings of the 300 and other reflections confirm the visual observations of the relative randomness of crystal orientation in a plane perpendicular to their c-axis. × 2.
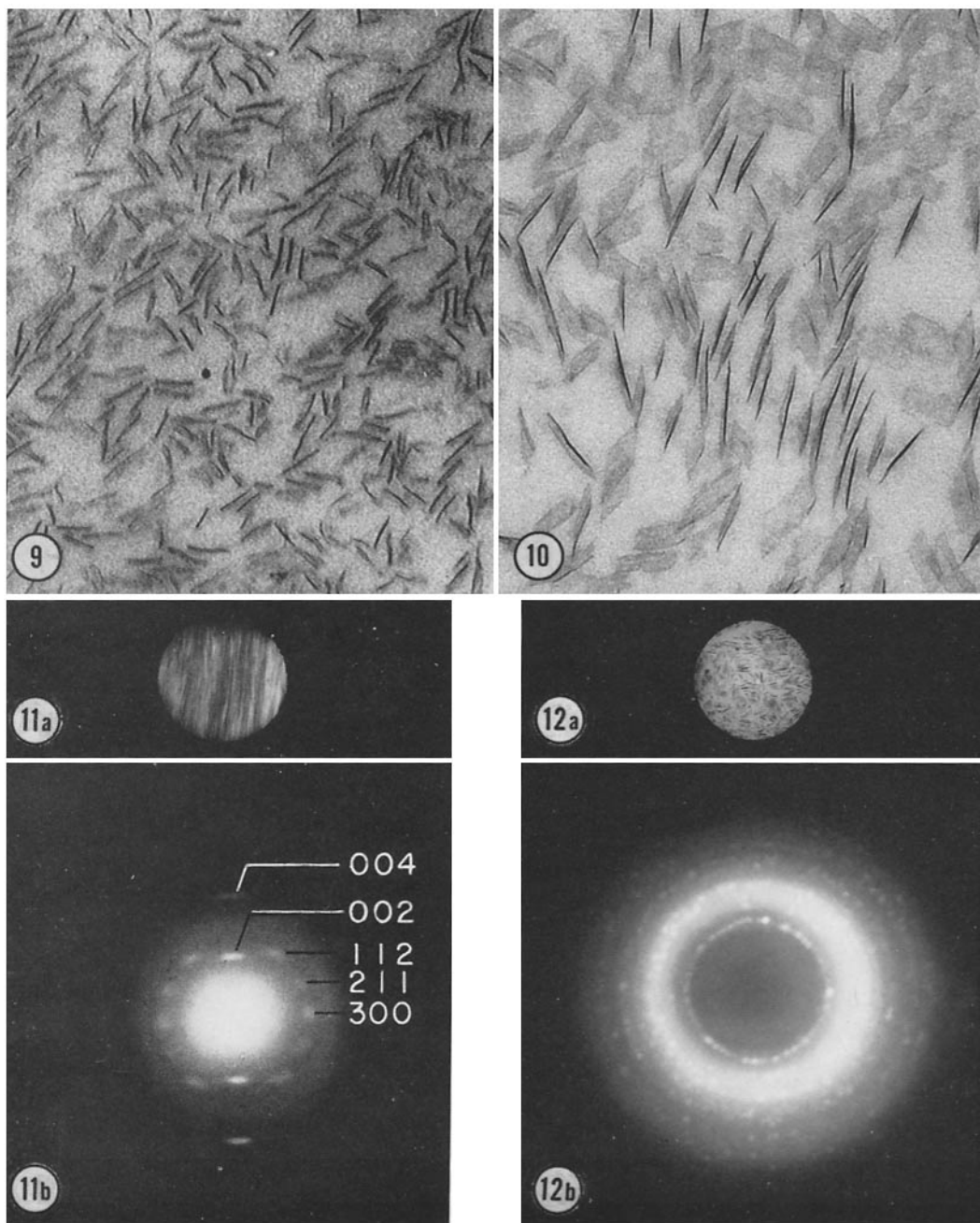
004
002
112
211
300

TABLE V

A Summary of the Significance of Differences in Crystal Dimensions of the Three Regions of Enamel

Dimension	Regions of enamel compared	Number of crystals measured	Mean dimension ± standard error of mean	t values	Probability values
			A		
Thickness	AEJ	142	19 ± 1	8.040	<0.01
	Midway AEJ-EDJ	53	100 ± 3		
	AEJ	142	19 ± 1	2.956	<0.01
	EDJ	48	167 ± 7		
	Midway AEJ-EDJ	53	100 ± 3	1.161	0.2–0.3
	EDJ	48	167 ± 7		
Width	AEJ	53	381 ± 25	0.0132	>0.9
	Midway AEJ-EDJ	24	395 ± 27		
	AEJ	53	381 ± 25	0.1180	>0.9
	EDJ	15	554 ± 29		
	Midway AEJ-EDJ	24	395 ± 27	0.1012	>0.9
	EDJ	15	554 ± 29		
Length	AEJ	29	1212 ± 232	0.001	>0.9
	Midway AEJ-EDJ	24	1095 ± 74		
	AEJ	29	1212 ± 232	0.005	>0.9
	EDJ	29	1629 ± 142		
	Midway AEJ-EDJ	24	1095 ± 74	0.020	>0.9
	EDJ	29	1629 ± 142		

cross-bridges in the organic matrix of embryonic human enamel (46, 47), cross-bridges connecting the thin filaments of the intraprismatic matrix were rarely observed in longitudinal prism profiles in this study. When observed, they were primarily seen at the AEJ in regions not well fixed by formalin before decalcification (Figs. 15 and 17). How-ever, patterns suggesting cross-bridges were frequently observed in the organic matrix when demineralized without prior treatment with formalin (17, 21).

STRUCTURE OF THE WALLS OF COMPARTMENTS

In longitudinal sections of the prisms, the 48 A

FIGURE 13 A partially decalcified section near the AEJ following uranyl acetate staining. The stippled material (*SM*) near the ameloblast-cell surface is continuous with the organic matrix. Note that both the stippled material and the organic matrix uncovered by partial demineralization with uranyl acetate staining have the appearance of short, swollen, fragmented filaments. Epon. × 51,200.

FIGURE 14 A higher magnification of a portion of Fig. 13, showing more clearly the short, swollen, fragmented filaments of both the matrix and the stippled material following uranyl acetate staining. Epon. × 128,000.

13

SM

14
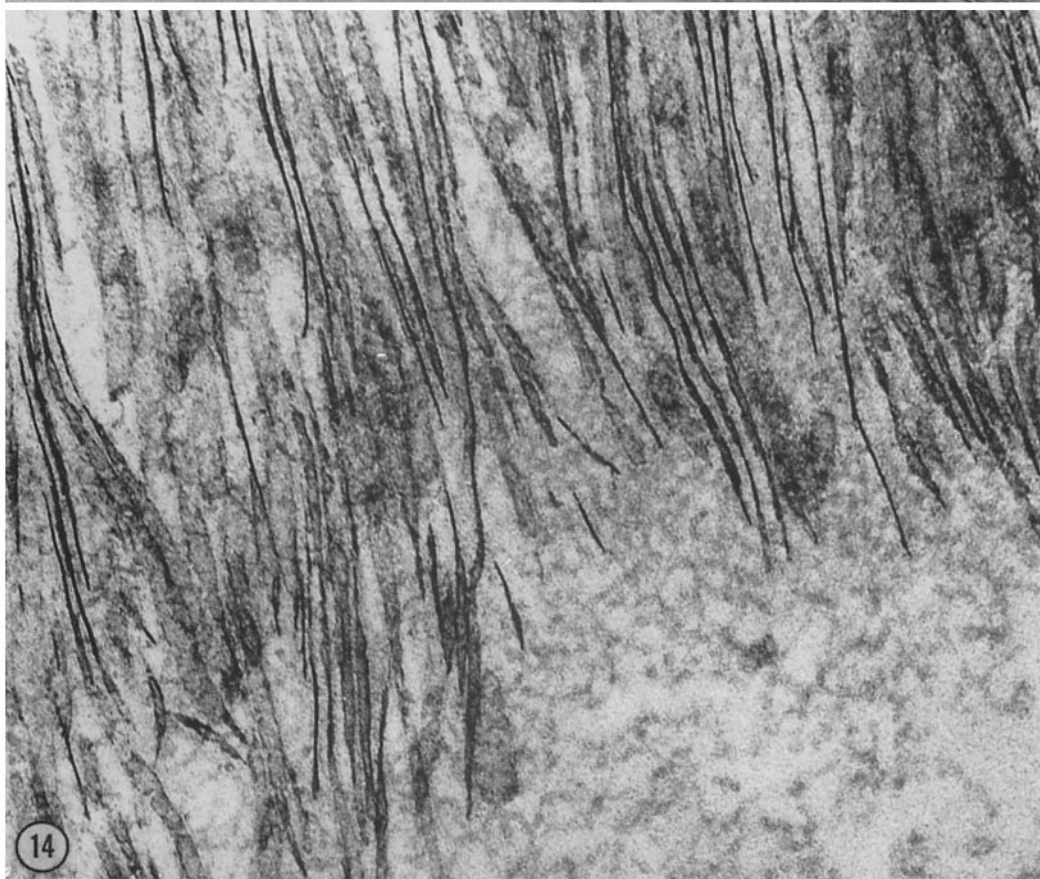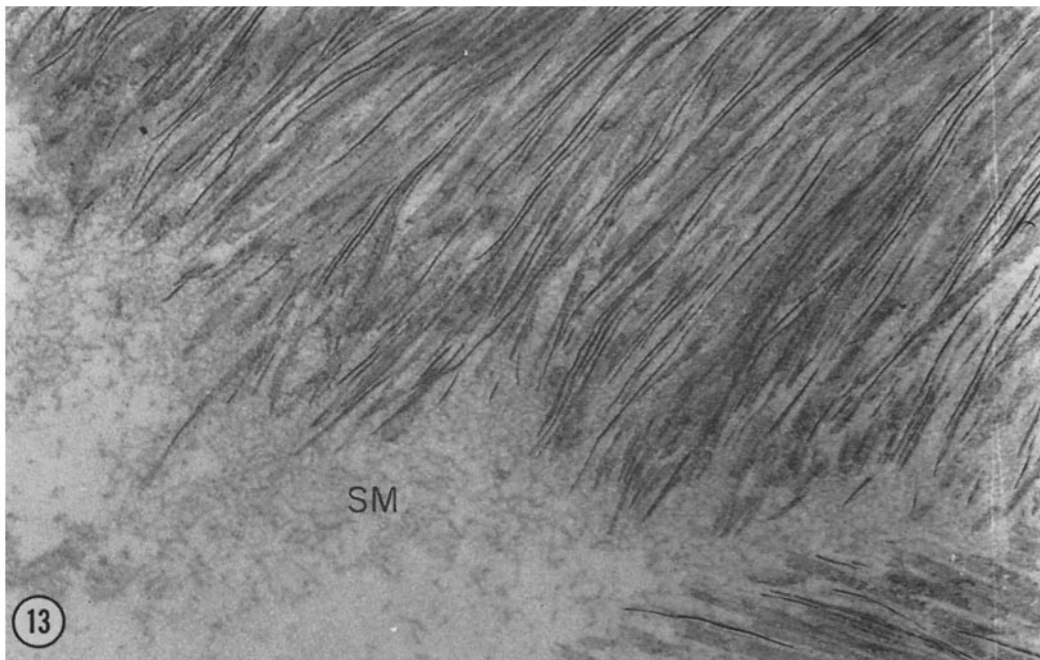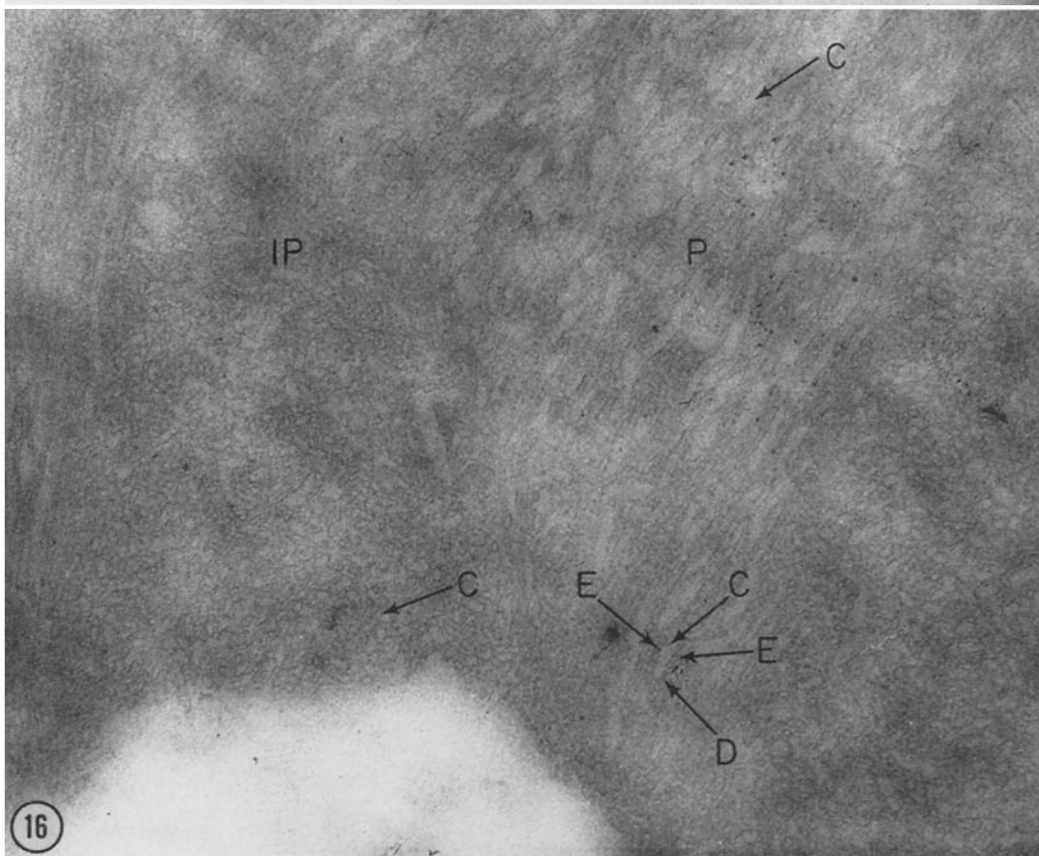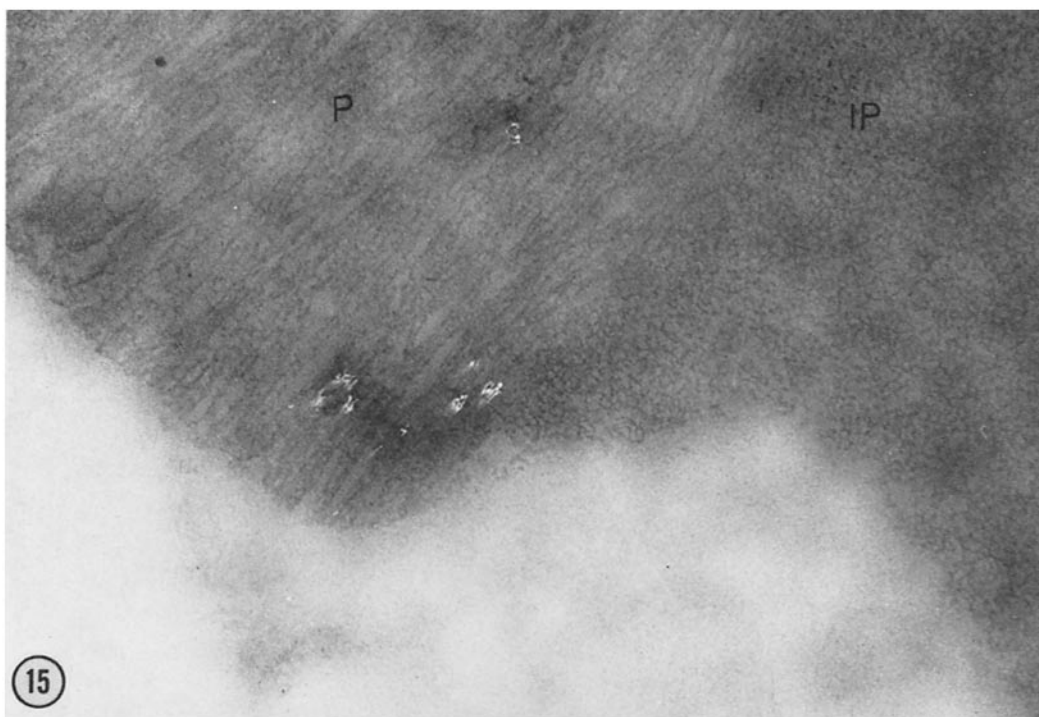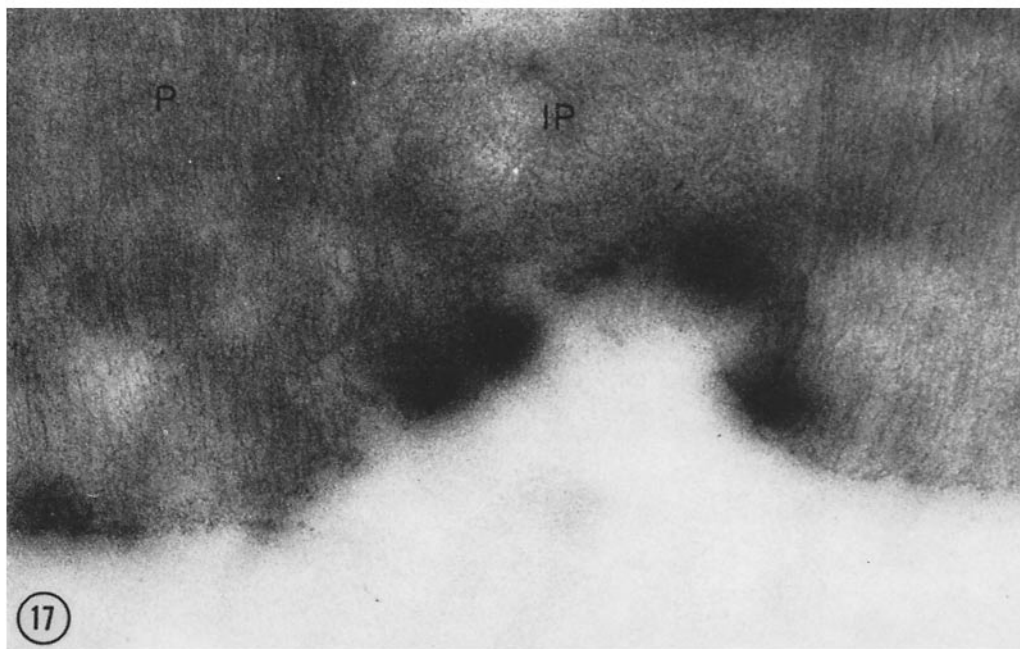
FIGURES 15, 16, and 17 Unstained decalcified sections of the organic matrix of enamel at the AEJ. In longitudinal or slightly oblique prism profiles (P), note that the intraprismatic organic matrix consists of a number of thin (48 A) dense lines having the appearance of filaments. In many regions these are organized into doublets (arrows D), the two individual filaments being separated by approximately 120 A. In addition, in the slightly oblique sections (Fig. 16, P), the organization of the intraprismatic matrix into compartments (arrow C) is evident. Note that in several regions the compartments are delineated by the 120 A doublets (arrows E). The oval or near oval compartments are more clearly observed in cross- or near cross-sections (arrows C) (Fig. 16, IP). Note the apparent occurrence of cross-bridge filaments in the longitudinal section of the prism (P) in Figs. 15 and 17 and the more filamentous or less obvious appearance of compartments in the IP region.

Such cross-bridge structures and the filamentous appearance of prism cross-sections were generally observed at the AEJ in sections not well fixed in formalin prior to demineralization. Methacrylate. × 64,000.

wide filaments were observed to consist of two dense lines, each approximately 12 A in width and separated by a less electron dense space of approximately 15 A to 17 A (Fig. 20 a and b. In) selected instances, the 12 A singlet also appeared to be composed of two single dense strands. In many longitudinal prism profiles there was a suggestion of an axial period of approximately 170 A (Figs 33 and 34). This was not observed in the filaments at the AEJ.

In cross-sections of the prisms, the subunits of the 48 A wide filaments were not observed. In most instances the wall of the compartments appeared to be a continuous structure or sheet. However, in several instances dot-like structures

approximately 48 A in diameter were also observed (Figs. 15, 16, and 36 a and b), and particularly at higher magnifications many of the sheets comprising this wall of the compartments appeared to be composed of a number of these closely packed dots rather than a continuous sheet.

PRISM SHEATHS

Surrounding either oblique or cross-sectional prism profiles is a region, approximately 425 A wide, which in mineralized sections is free of crystals. This region structurally separates one prism from the next and undoubtedly represents the prism sheath (Figs. 30 to 32, 35). The prism sheath is composed of many filaments, some of
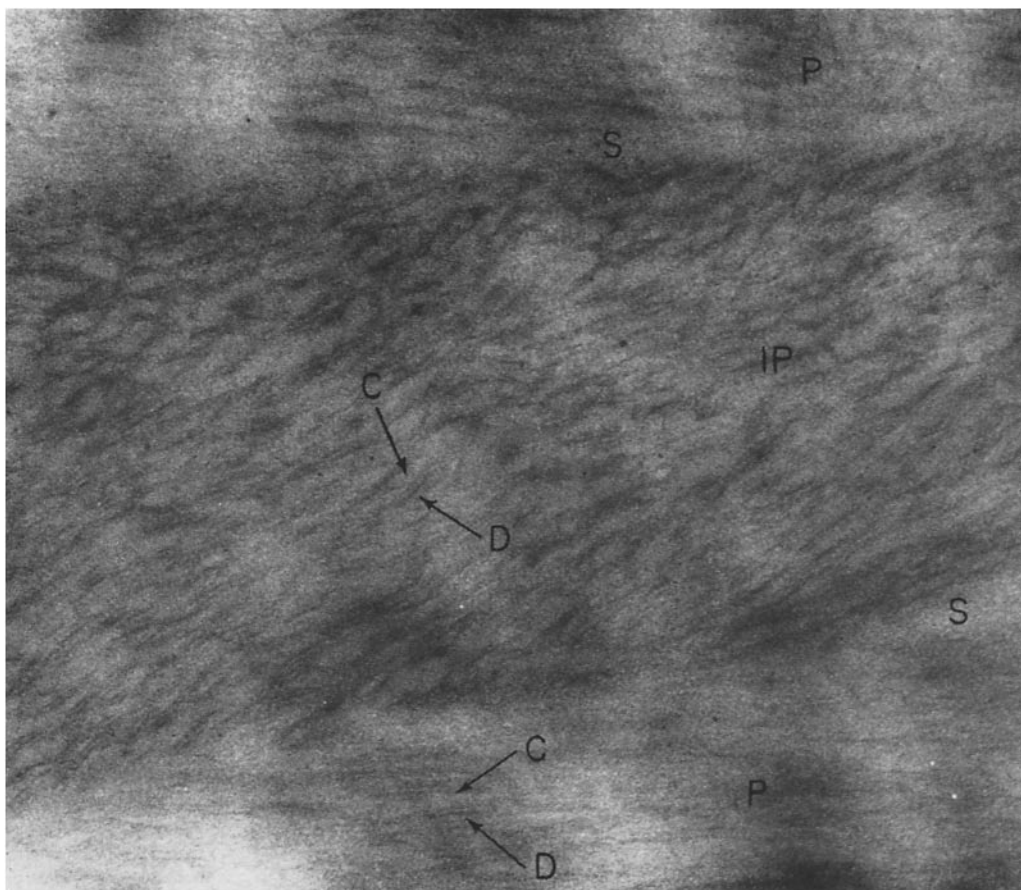
FIGURE 18   An unstained decalcified section near the AEJ, showing particularly an oblique prism profile. The doublet arrangement of the matrix filaments is clearly seen in both longitudinal and oblique sections. Spacing between the doublets is ∼120 A. In both the oblique (*IP*) and longitudinal prism profiles (*P*) the regions corresponding to the compartments (arrow *C*) are more clearly visualized to be delineated by the 120 A doublets (arrow *D*). There is some evidence in this section of a prism sheath (*S*) separating the *IP* profile from portions of the two longitudinal prism profiles on either side. Methacrylate. × 64,000.

FIGURE 19   A higher magnification of an unstained decalcified section of the enamel matrix at the AEJ. Note the thin, loosely packed filaments (48 A wide) which are organized into doublets. Spaces between the doublets average approximately 120 A. Methacrylate. × 128,000.

FIGURE 20   Fig. 20 *a* is a higher magnification of an unstained decalcified section showing a number of filaments seen near the AEJ. Note that where the doublet arrangement of filaments can be clearly observed in this section (arrows) each of the filaments is 48 A wide and is separated from the other member of the doublet by a space of approximately 120 A. Methacrylate. × 200,000.

Fig. 20 *b* shows that on closer examination of the filaments, each is composed of two dense strands of approximately 12 A (arrows) which are separated by a less electron-dense space of approximately 17 A. Methacrylate. × 1,080,000.

TABLE VI
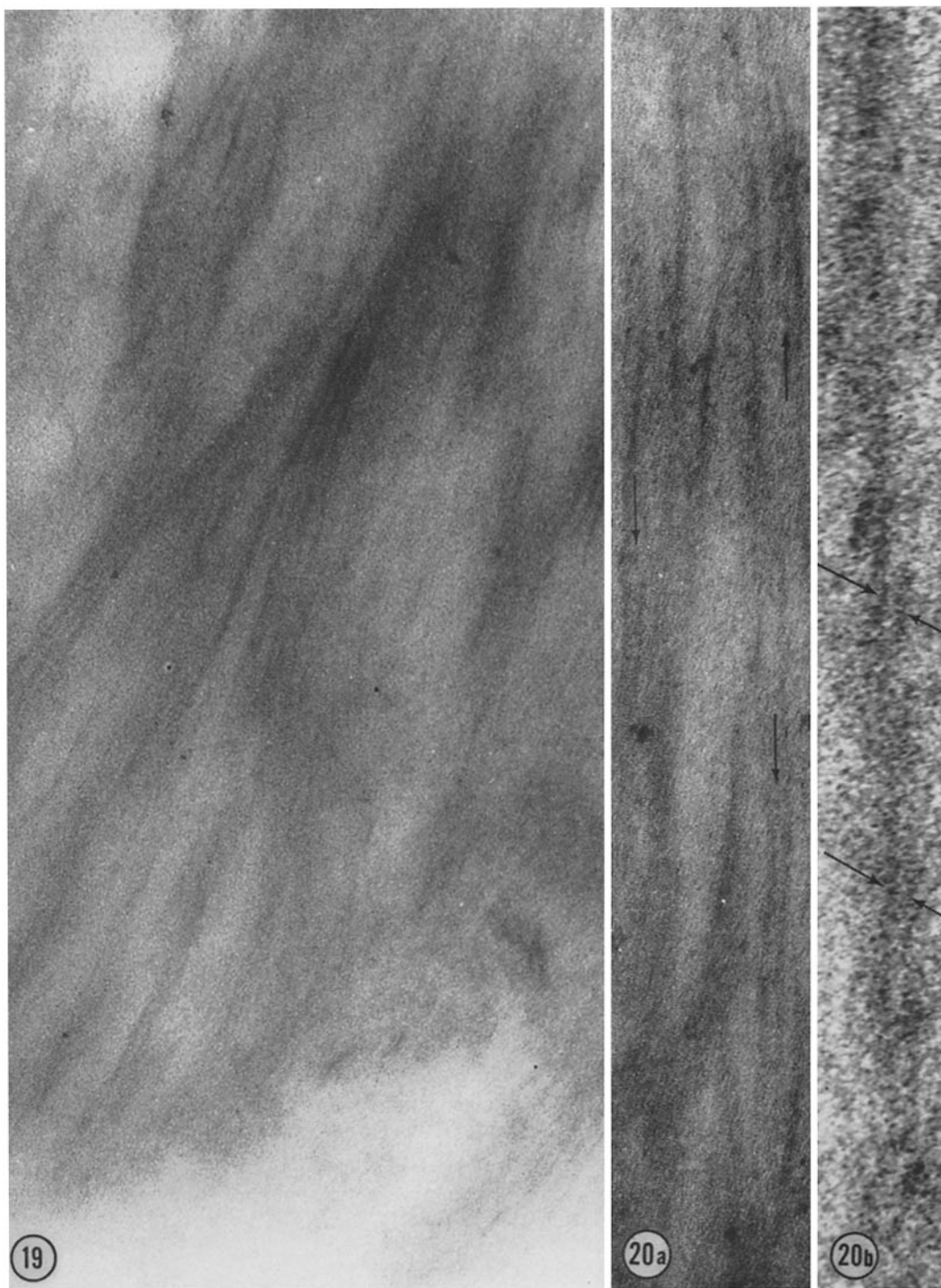
Measurements of Filaments and Spaces Between Filaments in Demineralized Enamel At and Near the AEJ

Number measured	Dimension	Mean value (range) A	Mean ± standard error of mean A
82	Total width of a filament	48 (30–78)	48 ± 2
99	Space between two filaments in doublet	122 (75–234)	122 ± 4
128	Width of a single strand of a filament	12 (4–23)	12 ± 1
61	Width of a space between two single strands composing a filament	17 (8–20)	17 ± 1
Calculated width of filament using 2 × mean value of single strand + width of space between 2 strands:		41	Difference between calculated and observed widths of filament: 7

TABLE VII

Measurements of Filaments and Spaces Between Filaments in Demineralized Enamel Midway Between the AEJ-EDJ

Number measured	Dimension	Mean value (range) A	Mean ± standard error of mean A
52	Total width of a filament	47 (35–78)	47 ± 2
89	Space between two filaments in a doublet	115 (75–200)	115 ± 3
135	Width of a single strand of a filament	12 (4–23)	12 ± 1
58	Width of a space between two single strands composing a filament	15 (8–20)	15
70	Spacing of periodic densities along filaments	169 (77–250)	169 ± 7

which run parallel to the prism axis, and others of which, intermeshed with them, run circumferentially around the prism perpendicular to the prism axis (Fig. 35). This arrangement of filaments in the prism sheath gives an appearance somewhat analogous to the cross-section of the walls of a wicker basket. A similar arrangement has been observed in prism cross-sectional profiles of decalcified enamel matrices from which some of the protein has been extracted (21). The prism sheaths, however, are not so clearly visualized in material prepared by demineralizing very thin sections of

FIGURE 21   Mineralized enamel midway between the ameloblast-enamel junction and the enamel-dentin junction (AEJ-EDJ). Note the marked improvement in general organization and architecture of the prisms, (P) and (IP); the much more closely packed and electron-dense crystals, and the increased degree of perfection of orientation of the long c-axes of the crystals paralleling the prism axis. Methacrylate. × 19,200.
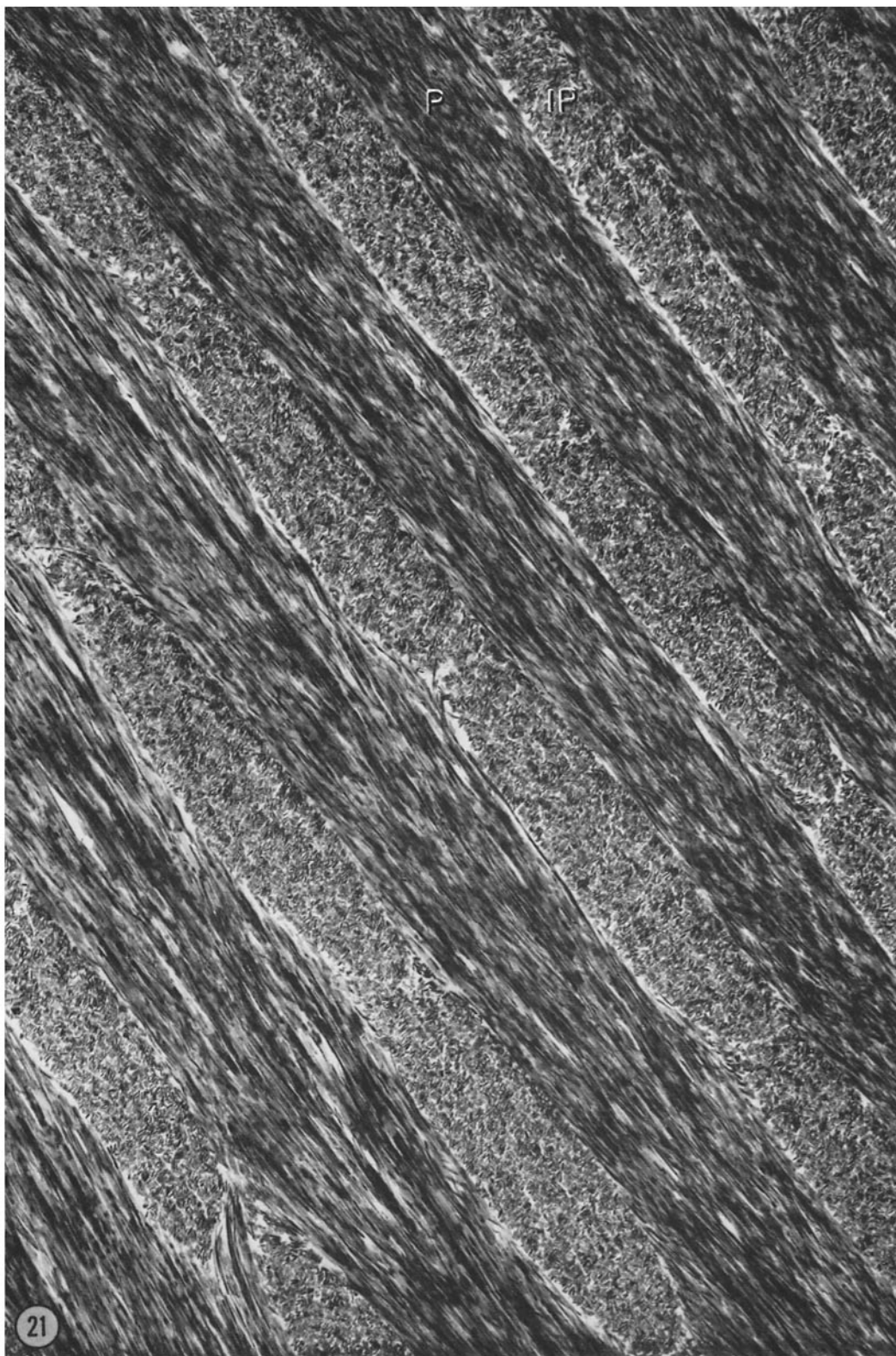
TABLE VIII

Measurements of Filaments and Spaces Between Filaments in Demineralized
Enamel Near the EDJ

Number measured	Dimension	Mean value (range)	Mean ± standard error of mean
		A	A
46	Total width of a filament	45 (30–75)	45 ± 2
121	Space between two filaments in a doublet	119 (75–156)	119 ± 2
105	Width of a single strand of a filament	12 (4–23)	12 ± 1
83	Width of a space between two single strands composing a filament	16 (8–20)	16
58	Spacing of periodic densities along filaments	188 (96–250)	188 ± 7

mineralized tissue as they are in thicker sections or in material demineralized prior to embedding (17, 21).

DISCUSSION

Inorganic Crystals

CRYSTAL SIZE, SHAPE, AND GROWTH

The youngest inorganic apatite crystals located near the AEJ are extremely thin plates whose thickness varies from approximately 9 A to a maximum of 35 A, with an average of approximately 19 A. The thinnest crystals are located in close approximation to the ameloblast cell surface. Rapid growth in thickness has occurred at approximately 1 μ above the cell surface, an observation similarly reported for developing human enamel (46, 47). Tables IV and V, which summarize the changes in crystal dimensions in the three regions of enamel studied, indicate that maturation of the crystals is accompanied primarily by an increase in thickness. The variability of crystal width and length measurements is un-

doubtedly due to the unavoidable errors involved in their measurement, as previously discussed, rather than to an inherent variation in the true dimensions of the crystals as deduced by statistical analysis (Table V).

Comparison of either the width or length measurements of the crystals by statistical analysis shows that there is no significant change in either of these dimensions in any given region. However, particularly in the case of the width measurements, the small number of crystals counted and the difficulties inherent in measuring true width dimensions undoubtedly leads to a larger spread or variation in this dimension. This makes it impossible to state definitively that crystal maturation is not, in fact, accompanied by some growth in crystal width. Statistically, however, the data obtained from this study do not permit the conclusion that growth in width has occurred (Table V).

Averaging the mean crystal width and length measurements obtained from each of the three enamel regions studied, one obtains a value of 400 A for crystal width and of 1300 A for crystal length, which closely approximates the dimensions reported in the enamel of human, hippopotamus,

FIGURE 22 A higher magnification of mineralized enamel midway between the AEJ-EDJ, showing the well organized prisms containing closely packed crystals. In the longitudinal prism profiles (P) the long axes of the crystals are clearly observed to be oriented parallel to the prism axis. Note that in the oblique prism profile (IPA) the crystals are oriented somewhat parallel to one another, while in the near cross-section prism profiles (IPB) the crystals are randomly oriented. Methacrylate. × 44,800.
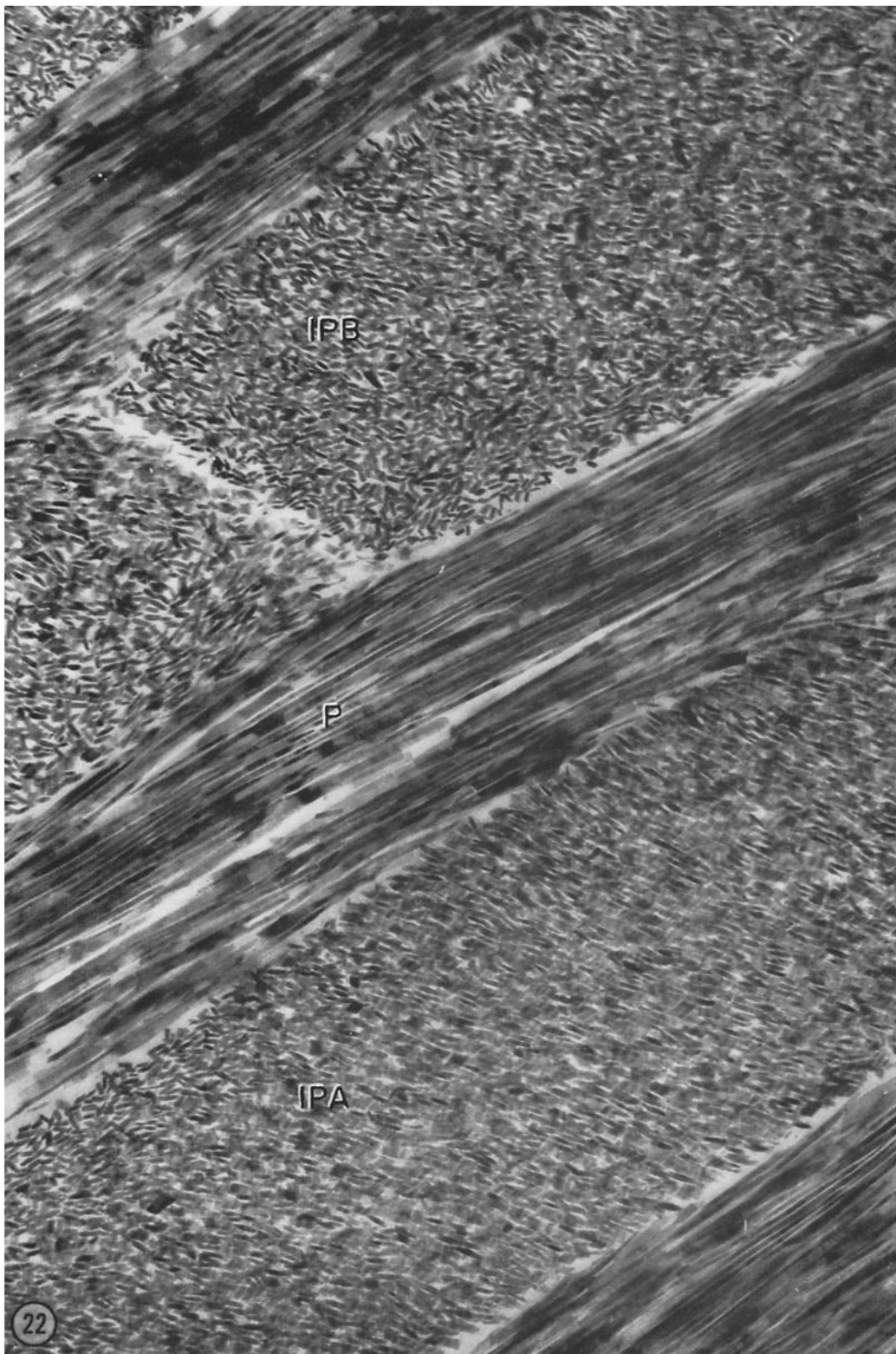
TABLE IX

A Summary of the Significance of Differences in Filaments and Spaces Between Filaments (Doublets) of Three Regions of Demineralized Enamel

Dimension	Regions of matrix compared	Number measured	Mean dimension ± standard error of mean	t values	Probability values
			A		
Total width of a filament	AEJ	82	48 ± 2	0.138	0.8–0.9
	Midway AEJ-EDJ	52	47 ± 2		
	AEJ	82	48 ± 2	0.400	0.6–0.9
	EDJ	46	45 ± 2		
	Midway AEJ-EDJ	52	47 ± 2	0.273	0.7–0.8
	EDJ	46	45 ± 2		
Space between two filaments in a doublet	AEJ	99	122 ± 4	0.280	0.7–0.8
	Midway AEJ-EDJ	89	115 ± 3		
	AEJ	99	122 ± 4	0.125	0.9
	EDJ	121	119 ± 2		
	Midway AEJ-EDJ	89	115 ± 3	0.346	0.7–0.8
	EDJ	121	119 ± 2		
Width of a single strand of a filament	AEJ	128	12 ± 1	0.00	>0.9
	Midway AEJ-EDJ	135	12 ± 1		
	AEJ	128	12 ± 1	0.00	>0.9
	EDJ	105	12 ± 1		
	Midway AEJ-EDJ	135	12 ± 1	0.00	>0.9
	EDJ	105	12 ± 1		
Spacing of periodic densities along filaments	Midway AEJ-EDJ	70	169 ± 7	0.199	0.8–0.9
	EDJ	58	188 ± 7		

FIGURE 23   A mineralized section of enamel midway between the AEJ-EDJ, showing a single longitudinal prism profile (*P*), in which the long axes of the crystals are clearly seen to be oriented parallel to the prism axis. Furthermore, there is a random orientation of the crystals around their long axes as is evident from the presence of both long wide crystal faces and long thick crystal faces in the same prism. The random orientation of crystals around their long axes is similarly seen in nearly cross-sectional prism profiles (*IP*). Note prism sheaths (*S*) which are free of crystals. Epon. × 38,400.
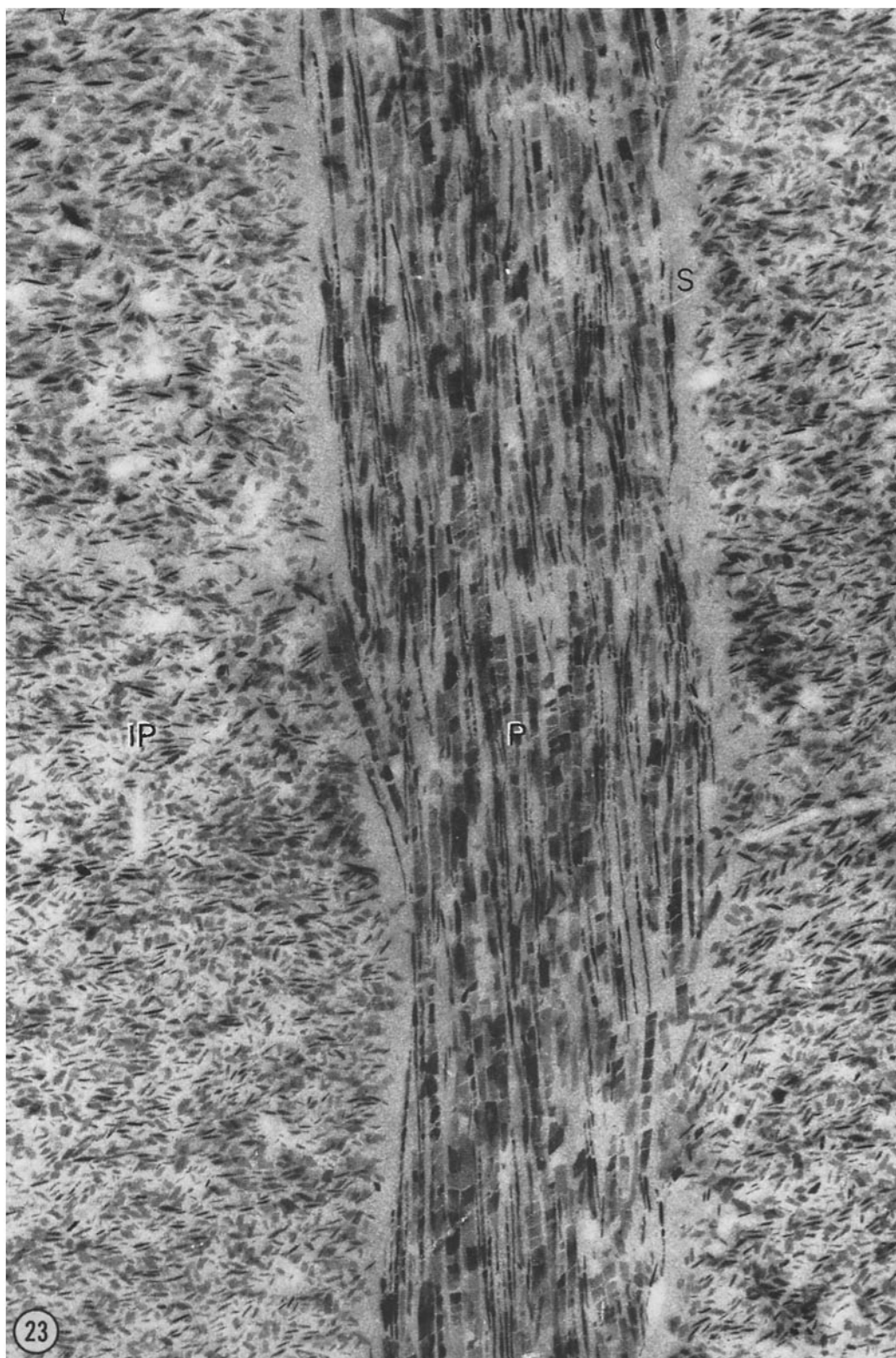
TABLE X

A Summary of the Significance of the Differences in Compartment Dimensions in Cross-Sections of the Intraprismatic Organic Matrix

Dimension	Region	Number of compartments measured	Mean dimension	t values	Probability values
			A		
Thickness of Compartments	AEJ	124	174 ± 7	0.318	0.7–0.8
	Midway AEJ-EDJ	70	252 ± 14		
	AEJ	124	174 ± 7	0.399	0.6–0.7
	EDJ	49	353 ± 20		
	Midway AEJ-EDJ	70	252 ± 14	0.169	0.8–0.9
	EDJ	49	353 ± 20		
Width of Compartments	AEJ	81	563 ± 32	0.089	>0.9
	Midway AEJ–EDJ	51	785 ± 38		
	AEJ	81	563 ± 32	0.094	>0.9
	EDJ	46	1262 ± 80		
	Midway AEJ-EDJ	51	785 ± 38	0.061	>0.9
	EDJ	46	1262 ± 80		

and rat (12, 34, 46, 47). The difference between the crystal length observed in this study and the extremely long lengths reported by Robinson (42), Watson and Avery (65), Fearnhead (7, 8), and others, in man, hamster, man, and rat, respectively, may be the result of the inherent errors and difficulties involved in the accurate measurement of this crystal dimension.

Although growth in crystal thickness alone has also been reported by Rönnholm (46, 47) during maturation of human enamel crystals, Nylen *et al.* (34) found that crystal growth in rat enamel includes a gradual increase in both width and thickness. Since the span of crystal maturation studied in the rat enamel covered a far greater range than either the present study or that reported in human

enamel (46, 47), the results are not completely comparable, and growth in crystal width may eventually occur in both bovine and human enamels in later stages of development.

The same may be true of the differences noted as regards the shape of the crystals. Nylen *et al.* (34) have clearly shown hexagonal profiles in cross-sections of crystals of the relatively mature enamel of rat. On the other hand, the present study, as well as one on more mature, developing embryonic *bovine* enamel in central incisor teeth (17), and studies on developing human enamel (46, 47) have indicated that the crystals have a rectangular cross-sectional profile. Further studies on fully mature, erupted bovine enamel are required in order to ascertain whether or not growth of the

FIGURE 24 A mineralized section of enamel in a region approximately midway between the AEJ-EDJ. This micrograph shows the varying angles at which the prisms are cut when the plane of section passes through regions in which some of the prisms take a wavy course through the enamel. Epon. × 12,800.

FIGURE 25 A mineralized section of enamel near that depicted in the previous figure. Figs. 24 and 25 point out that what appears as oblique or cross-sectional prism profiles in one view may appear as longitudinal prism profiles in another view. Epon. × 12,800.

D. F. TRAVIS AND M. J. GLIMCHER *Organic Matrix and Inorganic Crystals of Enamel*   **475**
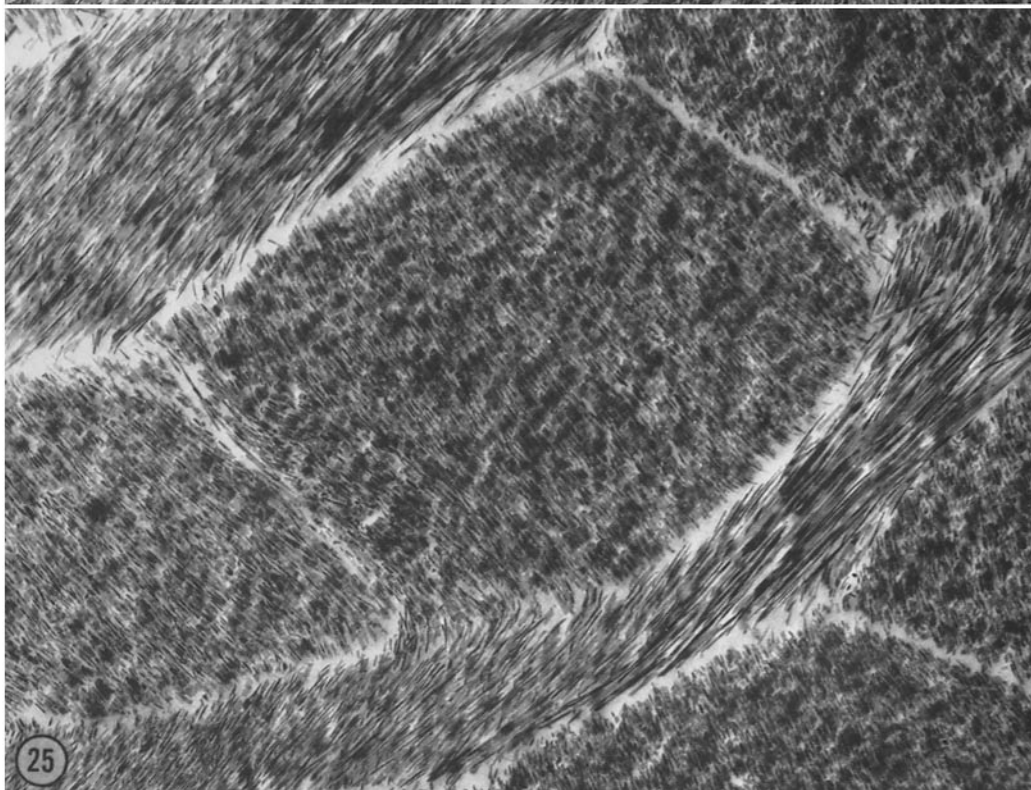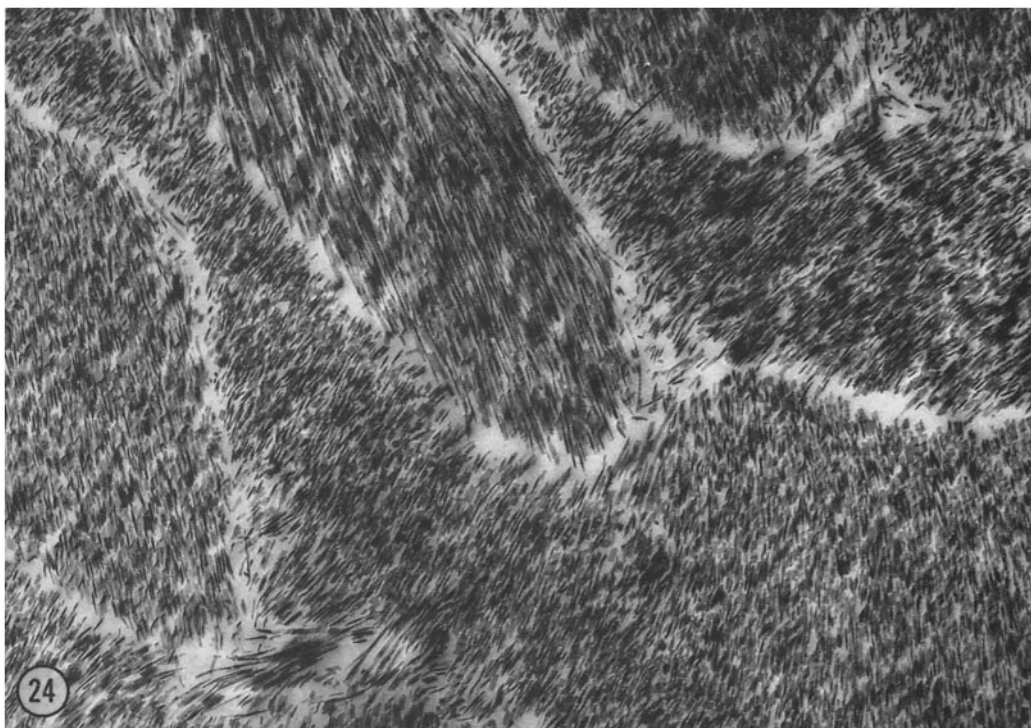
crystals in this tissue also results in a change in crystal habit with further maturation. In any event, whether the cross-sectional profile of the crystal is hexagonal or rectangular, the aforementioned studies, in addition to those of Johansen and Parks (24), Fearnhead and Elliott (9), and others, show that the cross-sectional profile is characterized by having one dimension (width) 2 to 4 times larger than the other (thickness); that is, the crystals are plates rather than equilateral hexagonal rods (10).

The earliest observable mineral crystals, identified as apatite by selected area electron diffraction, are the long, very thin plates similar in size and shape to those reported in developing enamel of other species previously mentioned. The small, round, discrete particles impregnating the enamel filaments, as depicted by Frank, Sognnaes, and Kern (10), were not observed. However, if the organic matrix does participate in crystallization by providing sites for nucleation as has been proposed for bone and cartilage (13, 14, 19, 23, 30, 31, 43, 44, 50, 51) there could be a relatively short transient period, during early nucleation and crystal growth, in which only very small crystals would be observed in direct relation to the filaments. Similar small, dot-like crystals have been seen during the earliest phases of crystallization of collagen in vivo (23, 32) and in vitro (13).

The significance of the electron-opaque line which essentially bisects the thickness dimension of the more mature crystals, in both longitudinal and cross-section profiles, is not readily apparent. Rönnholm (46) was able to observe this structure in addition to an electron-lucent line in the very youngest crystals (the latter of which was not observed in this study) only after burning them. He therefore suggested that it might reflect differences in the composition of the central and peripheral parts of the crystals or be due to embedded organic matrix between fused crystals. Nylen et al. (34) believed the observations were due to interference pattern effects. However, in the present study, the electron-opaque lines were seen to bisect the thick dimension of the crystals in both longitudinal and cross-sectional profiles without burning and at true focus. It is interesting to note that the width of this electron-opaque line is approximately 19 A, similar to the thickness of the young crystals at the AEJ region. Since the growth of the crystals is primarily confined to the thickness dimension, it is possible that, once the initial over-all habit of the crystal is reached by a relatively rapid initial period of crystal growth, further crystal growth occurs more slowly on the broad surfaces, and that this secondary growth phase introduces either a discontinuity, dislocation, or other lattice defect at the interface as a result of some imperfection or as a result of a change in the crystal structure of the newly deposited solid phase at the crystal surface. As pointed out by Nylen et al. (34), crystal growth undoubtedly occurs by the addition

FIGURE 26 Mineralized enamel midway between the AEJ-EDJ. The arrows show the electron-dense line which bisects the long thick dimensions of the crystals. Also see Figs. 37 and 38. Epon. × 180,000.

FIGURE 27 Mineralized enamel midway between the AEJ-EDJ, showing the electron-dense line which bisects the thick dimension of the crystals in near cross-section. Epon. × 171,000.

FIGURES 28 and 29. Selected area electron-diffraction patterns from crystals in both longitudinal and cross-sectional prism profiles midway between the AEJ-EDJ. Methacrylate.

Fig. 28 a. Shows the image of the diffraction aperture over crystals in the longitudinal prism profile. × 18,000.

Fig. 28 b. Shows the selected area electron-diffraction pattern of crystals seen in Fig. 28 a, showing orientation of the c-axis. × 2.

Fig. 29 a. Shows the image of the diffraction aperture over crystals in near cross-sectional prism profile. × 18,000.

Fig. 29 b. Shows selected area electron-diffraction pattern of crystals seen in Fig. 29 a, indicating the random orientation of the crystals about their long axis. × 2.
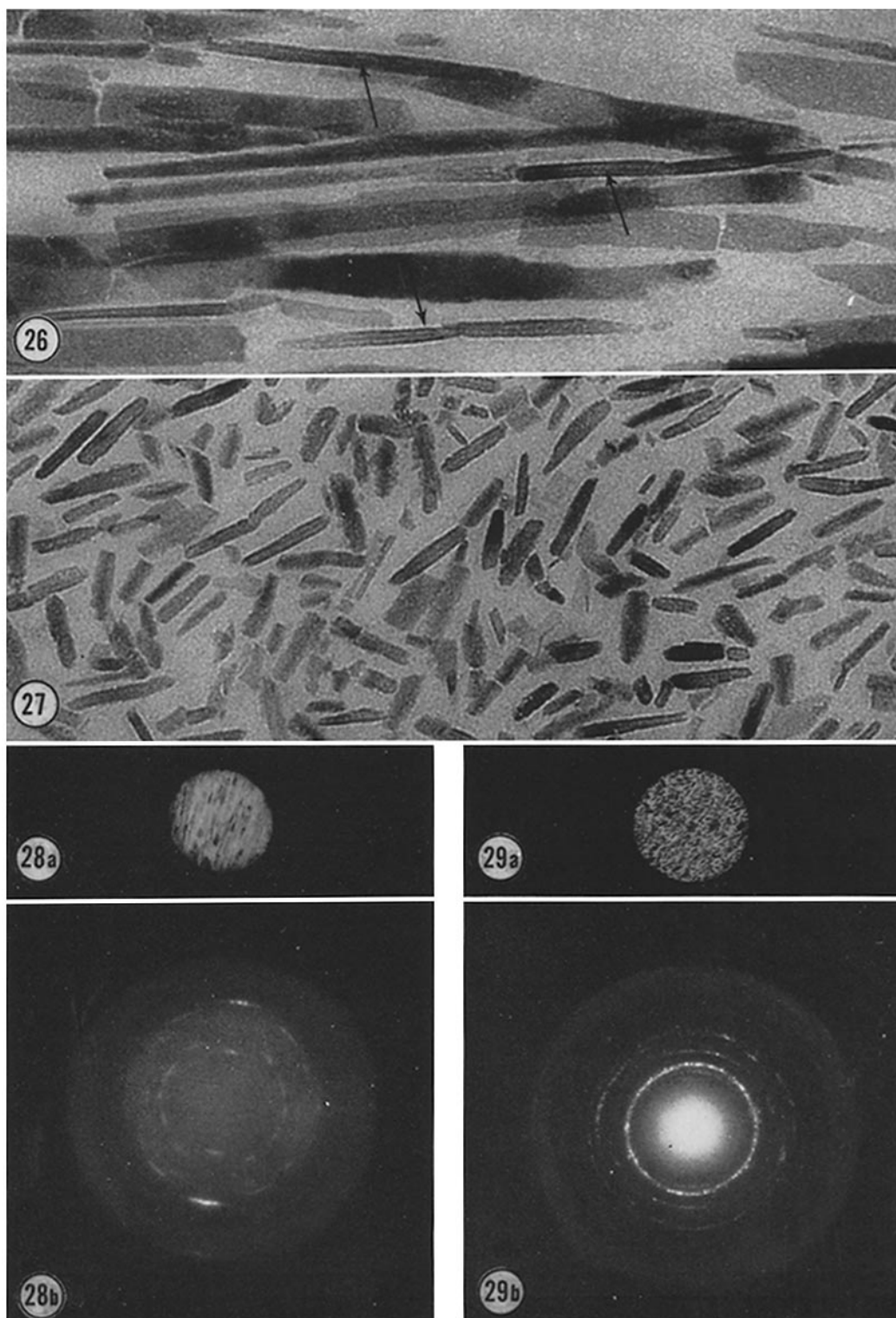
of lattice ions (either from the diffusion of extra-cellular fluid or from recrystallization, *i.e.* the growth of larger crystals at the expense of smaller crystals which are solubilized), rather than by actual physical fusion of adjacent crystals (46, 47).

ORGANIZATION OF THE PRISMS AND CRYSTALS

Although the width of prisms does not appreciably change from the youngest (AEJ) to the most mature (EDJ) regions, their organization and architecture becomes much more ordered. Concomitant with this increased degree of ordering of the prisms, the individual apatite crystals also become more closely packed and show an increase in the degree of perfection of orientation of their long axis parallel to the long axis of the prisms, also confirmed in a previous report on embryonic bovine central incisor teeth (17). Although the crystals are almost perfectly aligned with regard to their long axes, they are randomly rotated about their long axes. Likewise, the present study also confirms the results (17) that the crystals within a single prism are similarly oriented, and no evidence was found for two distinct sets of crystals, within a single prism, distinguished by their deviation from the long axes of the prisms (52). Furthermore, a high degree of perfection of the orientation of the *c*-axis of the crystals was found within a single prism, both visually and by selected area electron diffraction.

Organic Matrix

The organic matrix of developing embryonic bovine enamel is organized remarkably like that of mineralized enamel. We wish to emphasize that the treatment of thin mineralized sections (prepared for electron microscopy) with formalin prior to decalcification preserves the structure and organization of the organic matrix. This is evident from a comparison of such treated sections with untreated preparations (17, 21). In the latter there is extreme swelling of the entire prism by as much as tenfold, in contrast with the maintenance of prism size and organization in formalin-treated sections. Prisms in varying profiles are clearly observed in addition to the prism sheaths which surround and serve to separate adjacent prisms. In longitudinal prism profiles, the *intra*prismatic organic matrix appears as a series of thin (48 A) dense lines having the appearance of filaments. These filaments are relatively parallel to one another and to the long axes of the prisms within which they are located, an

organization closely paralleling the orientation of the long axes of the inorganic crystals.

Both cross- and oblique prism profiles clearly indicate that the *intra*prismatic organic matrix is organized as a series of relatively parallel *tubular sheaths* having an oval or nearly oval cross-sectional profile. Although the predominant feature of the cross-sectional compartment profiles is that their walls consist of a continuous *sheet*, dot-like structures similar in width to the dense lines (48 A wide) seen in longitudinal sections were also observed in the wall of the sheaths. Both structures, continuous sheets or a series of closely packed filaments, are consistent with the appearance of the intraprismatic matrix in longitudinal sections. X-Ray diffraction studies have indicated that the organic matrix proteins of embryonic bovine enamel are in a cross-β-configuration (15). Although proteins in β-configuration are usually aggregated in the form of pleated sheets, the model proposed for the embryonic enamel proteins (16) is also consistent with the view that the walls are composed of a series of closely packed and parallel filaments. This is a direct consequence of the unusually high content of proline in embryonic enamel proteins (5, 6, 16, 20, 39), and specifically in the fraction soluble in cold neutral buffer solutions (20) corresponding to the intraprismatic proteins (21). Preliminary model-building experiments indicated that such a high content of randomly distributed proline could be accommodated in a cross-β-structure by introducing a 180° bend in the polypeptide chain at each pyrrolidine residue (16). Because of the frequent occurrence of proline, the distance between the 180° bends is small. Therefore, the resultant structure, consisting of very narrow, anti-parallel, pleated sheets, would have the appearance of filaments if extended perpendicular to the direction of the polypeptide chains (16).

The regular appearance and shape of the compartments and the paucity of visible cross-bridges make it very unlikely that the compartments are formed by randomly dispersed sheets or as the result of a three-dimensional network of cross-bridged septa (46, 47).

The relative constancy of the 120 A doublet space observed in longitudinal sections from the AEJ to the EDJ and the appearance of this doublet and the compartments in oblique sections as well as in selected cross-sectional profiles strongly suggest that the doublets represent the distance be-

tween adjacent walls of the compartments. Viewed in this light, the spaces between adjacent doublets or between single 48 A wide filaments which are not observed as doublets in longitudinal and oblique sections probably represent the inside dimensions of the compartments.

The size of the compartments is more than ample to accommodate the inorganic crystals at any of the stages of development observed. Such a view is consistent with the observed random orientation of the cross-sectional profiles of the compartments and the random orientation of the crystals about their long axes. A similar conclusion was reached by Scott and Nylen (49), who felt that the organic structures observed in cross-sections of rat enamel conformed to the peripheral cross-sectional outlines of the crystals.

Both the apatite crystals and the tubular sheaths of the intraprismatic organic matrix are similarly oriented with their long axes relatively parallel to the long axes of the prisms within which they are located and randomly rotated about their long axes. Since there is evidence that the organic matrix is secreted by the ameloblasts prior to calcification of the enamel (64, 65), it would appear that the organization of the tubular sheaths plays a major role in the ordered arrangement of the inorganic crystals within the prisms. It is important to re-emphasize here that the process of preferential crystal orientation may be unrelated to the mechanism *inducing* crystallization, a situation similar to that suggested for bone and cartilage (13). As has been postulated in the case of bone, preferred orientation of the crystals is probably a function of the size, shape, and growth of the inorganic crystals in relation to the highly ordered packing and organization of the components of the organic matrix, rather than a true epitaxial growth (13).

The Prism Sheaths

The prism sheaths which surround the individual prisms appear to be composed of many filaments arranged in a basket-weave fashion, some of which run parallel to the prism axis, and others of which, intermeshed with them, run circumferentially around the prism perpendicular to the prism axis. The sheaths are not mineralized in either bovine embryonic premolar teeth of varying age or in more mature embryonic central incisor teeth (17). They are evident in mineralized sections as clear electron-lucent areas, free of crystals, which separate one prism from the next. The failure of the prism sheaths to mineralize may be a reflection of either a different basic molecular structure and/or organization of the protein or other components of the organic matrix, or the presence of other material which inhibits the deposition of mineral. In any event, this network of organic material may play a vital role in the diffusion of solutes and solvents through a tissue such as enamel, which is composed primarily of highly ordered and densely packed inorganic crystals.

FIGURE 30   An unstained decalcified section of the organic matrix of the enamel midway between the AEJ-EDJ. Note the increased degree of organization and architecture in the matrix over that observed at or near the AEJ. Both the longitudinal prism profiles (*P*) and the slightly oblique prism profiles (*IP*) are clearly defined. Also note that the thin filaments in longitudinal prism profiles are again visualized as doublets, are more closely packed, and are arranged parallel to the prism axis. Similarly, in the slightly oblique prism profiles (*IP*), note the presence of oval or near oval compartments. Methacrylate. ✕ 22,400.
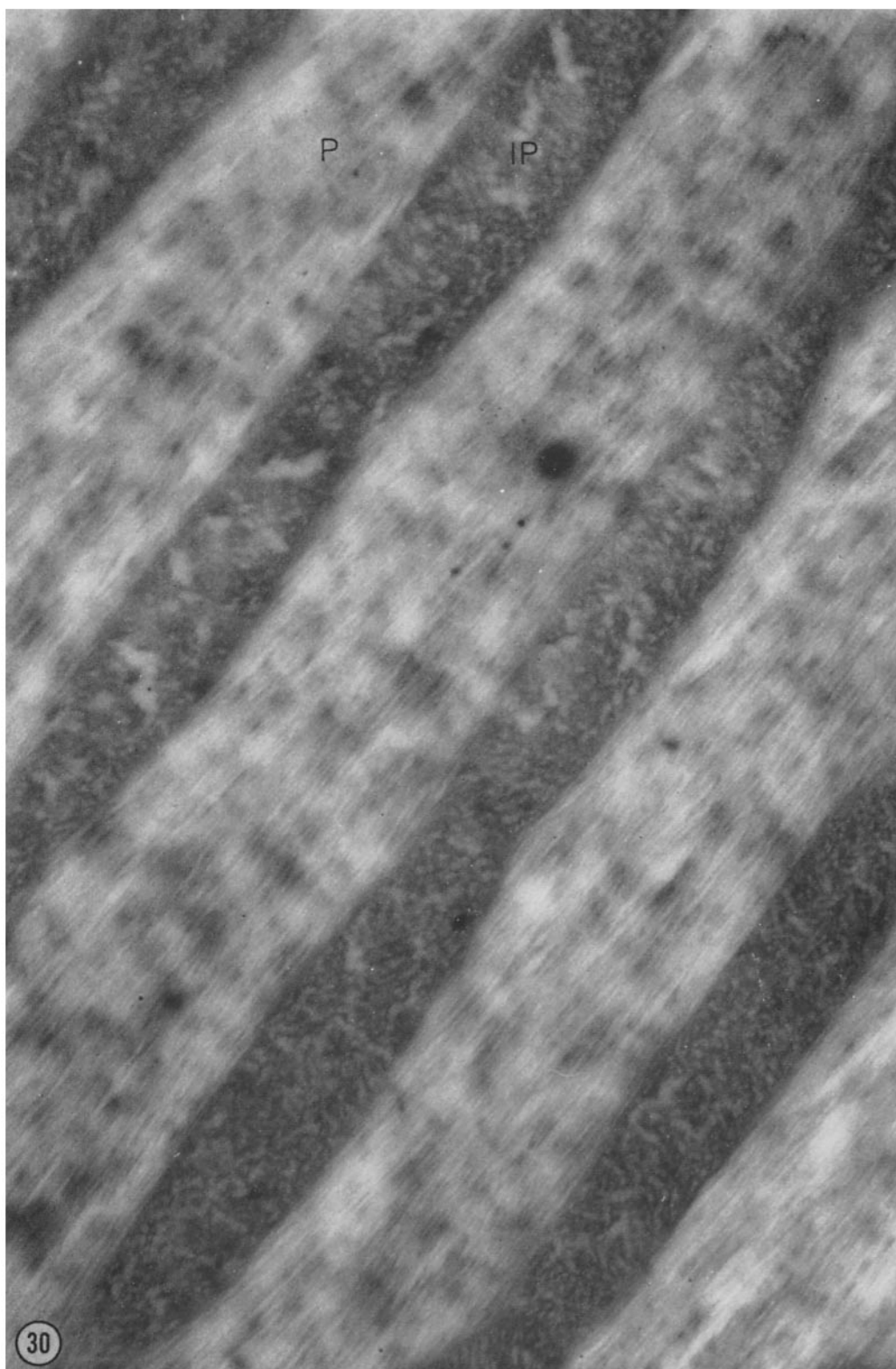
Figure 31   An unstained decalcified section of the enamel matrix midway between the AEJ-EDJ. Note the closely packed filaments arranged in doublets (arrows D) which parallel the long prism axis in (P), and the oval or near oval compartments (arrows C) in (IP). Methacrylate. $\times$ 38,400.

Figure 32   A uranyl acetate-stained decalcified section of the enamel matrix midway between the AEJ-EDJ. The closely packed filaments, arranged as doublets, parallel the prism axis. The spacing between the filaments composing a doublet is approximately the same as that at the AEJ. Also note the presence of the prism sheath (S) which separates the longitudinal prism from portions of the two oblique prisms. The sheath appears to be composed of many filaments, some of which run circumferentially around the prism while others run parallel to its axis, also seen in Fig. 36. Methacrylate. $\times$ 128,000.
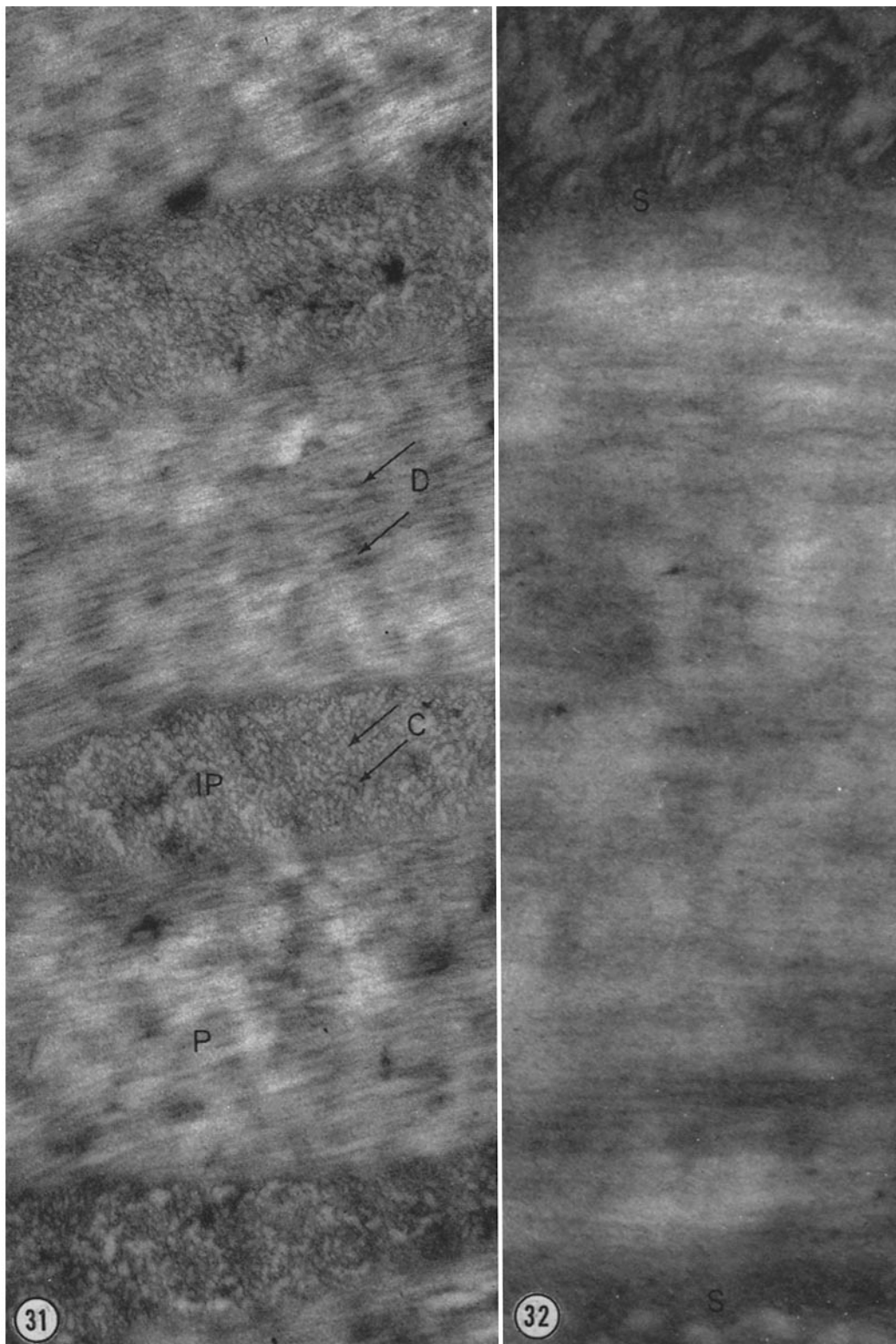
FIGURE 33 A portion of an unstained decalcified section of enamel matrix midway between the AEJ-EDJ. Note the arrangement of the filaments into doublets (arrow D). Each filament composing a doublet is separated by a space of ~120 A. There is also a suggestion of axial periods of approximately 170 A (vertical marks). Note the compartments (arrow C) between adjacent doublets (arrow D) or between single filaments and single filaments and doublets. Methacrylate. $\times$ 128,000.

FIGURE 34 A higher magnification of a portion of Fig. 33, showing the doublet arrangement of the filaments and the suggestion of axial periods along them. Also note that each filament of a doublet appears to be composed of two dense strands. Methacrylate. $\times$ 200,000.

FIGURE 35 A partially demineralized section of enamel midway between the AEJ-EDJ, clearly showing the prism sheath (S). Methacrylate. $\times$ 96,000.

D. F. TRAVIS AND M. J. GLIMCHER   *Organic Matrix and Inorganic Crystals of Enamel*   **485**
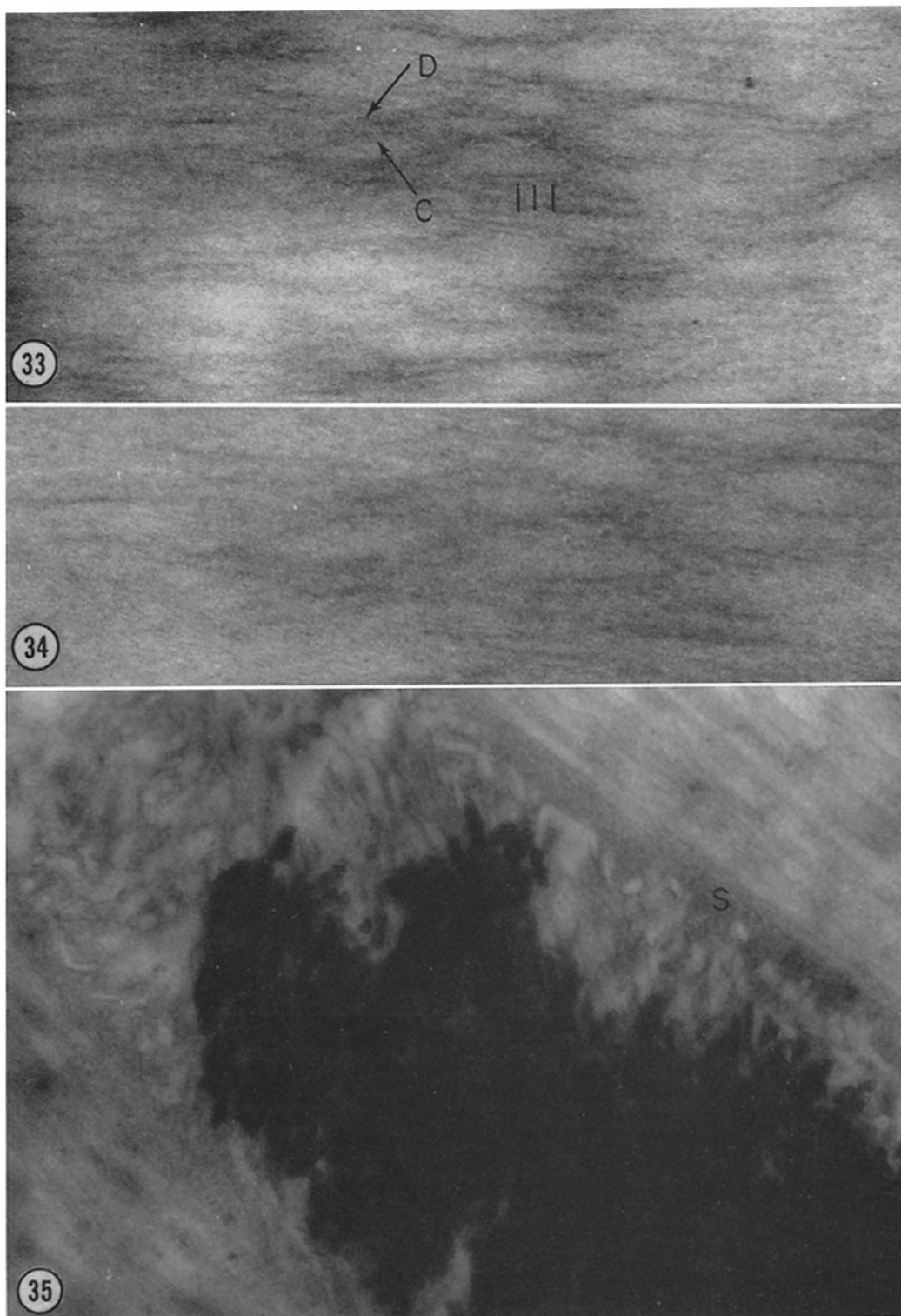
FIGURE 36 *a* and *b* Unstained demineralized cross- or near cross-sections of enamel prisms, showing the organization of the intraprismatic organic matrix into randomly oriented oval or near oval compartments (arrow *C*). The doublets or spaces between the individual compartments are in many instances separated by approximately 120 A, giving the appearance of a doublet (arrow *D*). This doublet undoubtedly corresponds to the doublet seen between the dense lines of filaments in longitudinal sections. The walls of the compartments are approximately 48 A thick, also corresponding to the width of the dense lines or filaments seen in longitudinal sections. The fine structure of the walls is predominantly that of a continuous sheet, although in several regions the walls appear to be composed of closely packed dots, 48 A wide (arrows *F*), suggesting that the walls are in fact not continuous sheets but consist of closely packed filaments. Methacrylate. Fig. 36 *a*, × 132,000; Fig. 36 *b*, × 156,000.
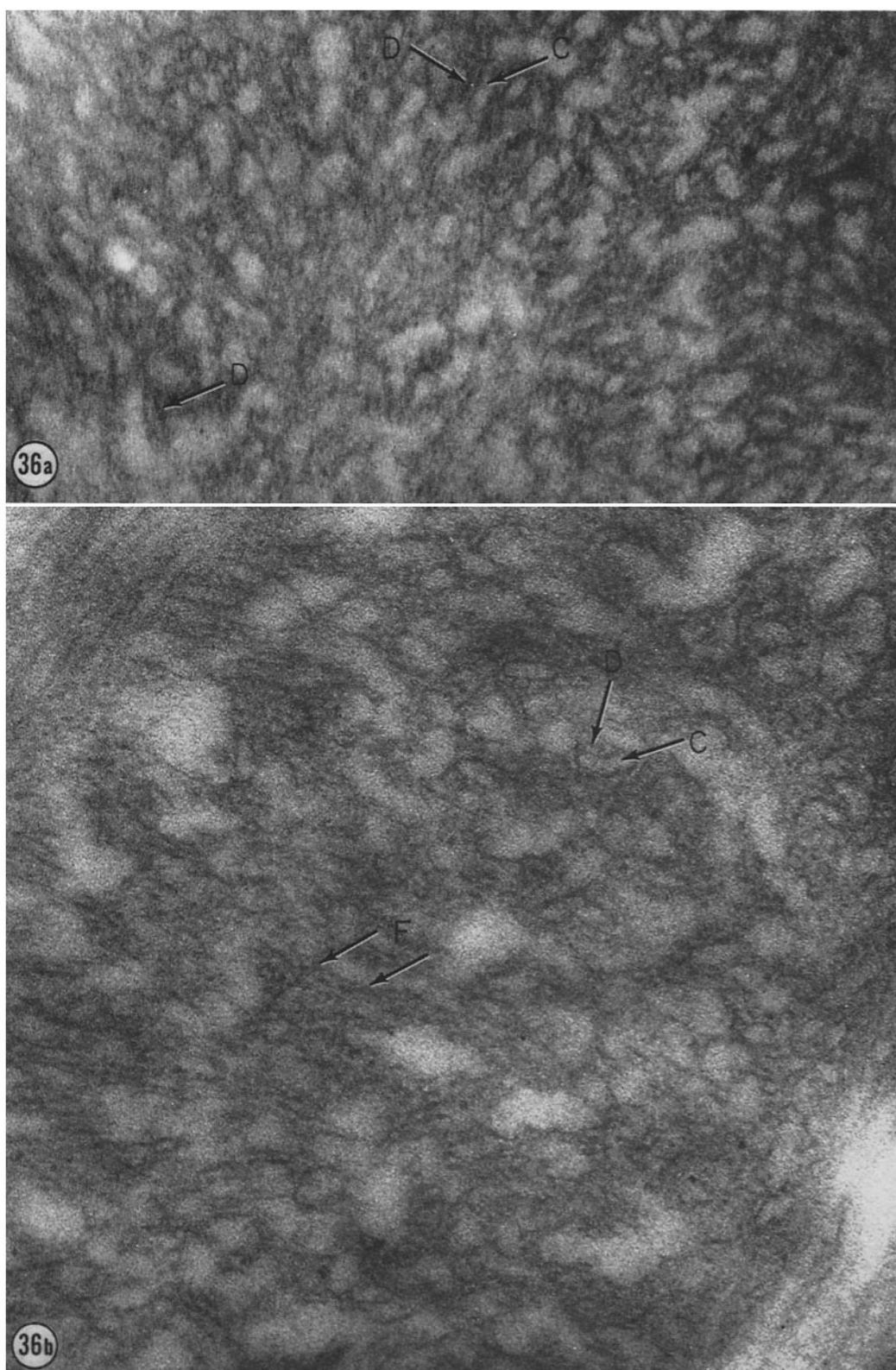
FIGURE 37   A mineralized section of enamel near the EDJ, showing typical moiré patterns (arrow *M*) which are frequently observed where two single crystals overlap at varying angles. Note the tapered edges on each end of the crystals as well as the low electron density demarcations between them when they are viewed in long broad profiles (arrows). Methacrylate. × 128,000.

FIGURE 38   A mineralized section of enamel near the EDJ, also showing moiré patterns frequently observed where two single crystals overlap at varying angles. The electron-opaque lines which bisect the long thick dimensions of the crystals are also seen (arrows). Epon. × 128,000.

FIGURE 39   A mineralized section of enamel near the EDJ showing the region, approximately 12 μ from it, at which the oblique and cross-sectional prism profiles terminate. Note the band of well defined enamel crystals, longitudinally oriented, wihch extend toward the EDJ as indicated by direction of the arrow. Epon. × 12,800.
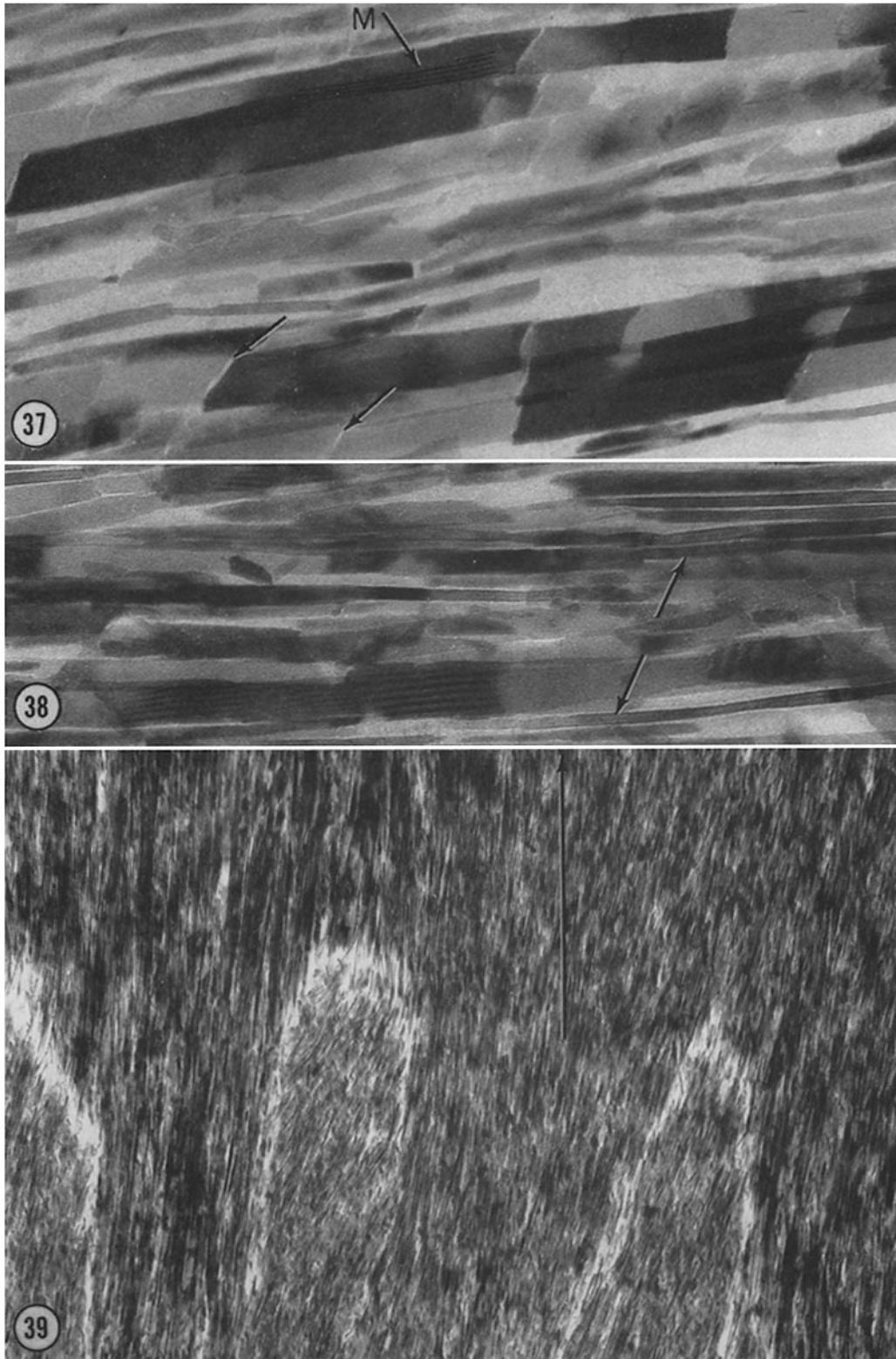
FIGURE 40 A mineralized section of enamel at the EDJ. Note the interdigitation of the enamel with the dentin. The dentin (D) is of lower electron density, contains smaller crystals, and is arranged in many regions with the axial spacing typical of collagen. Epon. × 38,400.

FIGURE 41 A mineralized section of enamel at the EDJ. Note that even in the interdigitations, where the general organization of prisms is lacking, the enamel crystals are oriented so that their long axes are roughly parallel to one another and to the general direction of the longitudinally dispersed crystals situated at the termination of the prisms (seen in Fig. 39). Epon. × 64,000.

FIGURES 42 and 43 Selected area electron-diffraction patterns from enamel crystals at the EDJ and of hydroxyapatite crystals in dentin. Methacrylate.

Fig. 42 a. Shows the image of the diffraction aperture over the enamel crystals diffracted at the EDJ. × 18,000.

Fig. 42 b. Shows the selected area electron-diffraction pattern from the region seen in Fig. 42 a. Note that the long dimensions of the crystals correspond to their c-axes. × 2.

Fig. 43 a. Shows the image of the diffraction aperture over the dentin at the EDJ. × 18,000.

Fig. 43 b. Shows the selected area electron-diffraction pattern from the region seen in Fig. 43 a. Note that from the same volume of tissue broader reflections are shown as well as complete rings. This confirms the visual evidence that the number of crystals per volume in dentin is considerably greater and that the apatite crystals in dentin are considerably smaller than those of enamel. × 2.
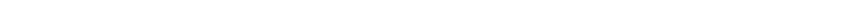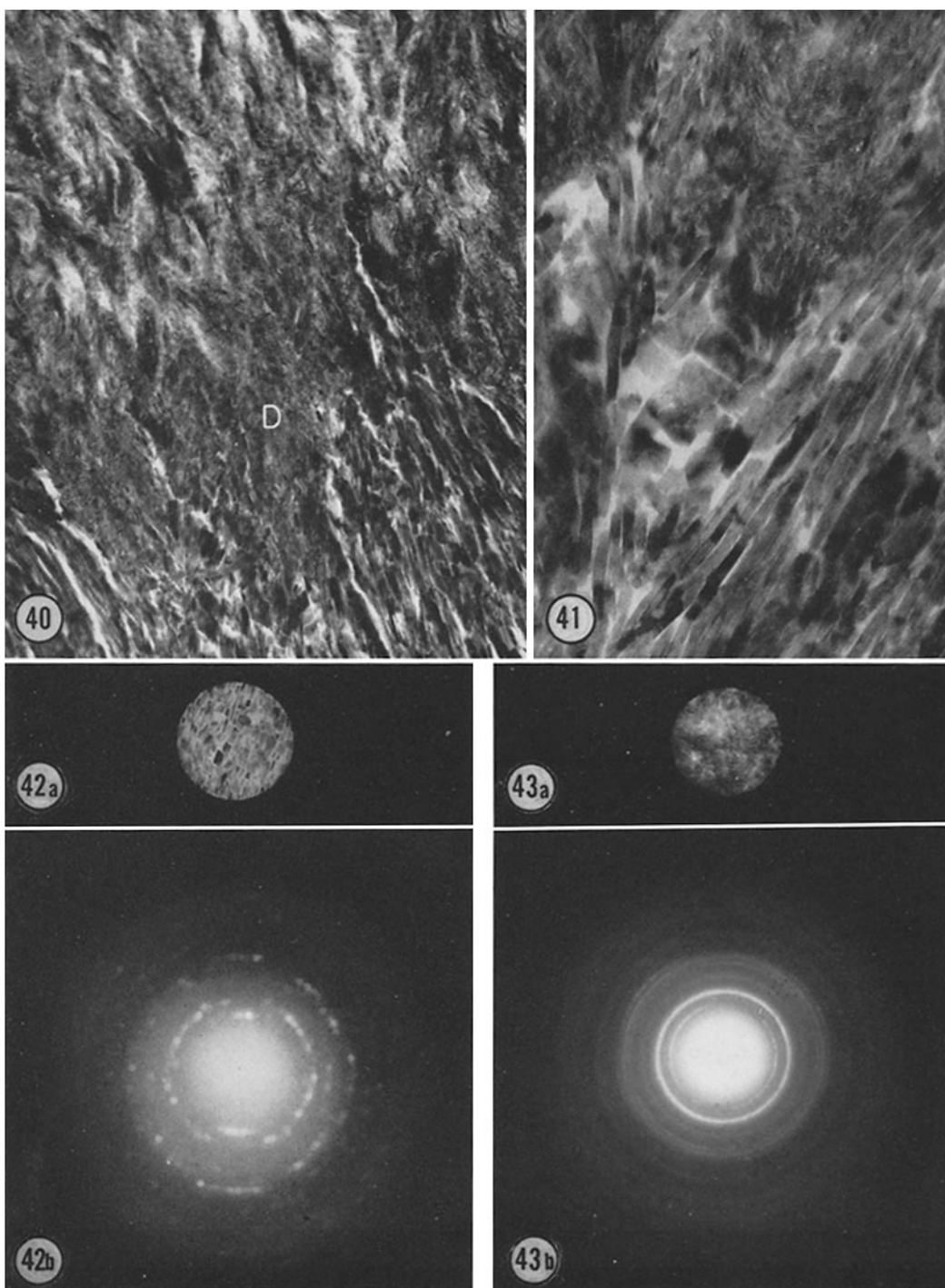
FIGURE 44   An unstained demineralized section of the enamel matrix near the EDJ in
which a longitudinal prism profile is shown with portions of two oblique prism profiles on
each side. Note the closely packed filaments, arranged as doublets, paralleling the prism
axis. The spacing between the filaments composing a doublet is ∼120 A as previously
noted. Also note the suggestion of an axial period along the filaments. Methacrylate.
× 128,000.

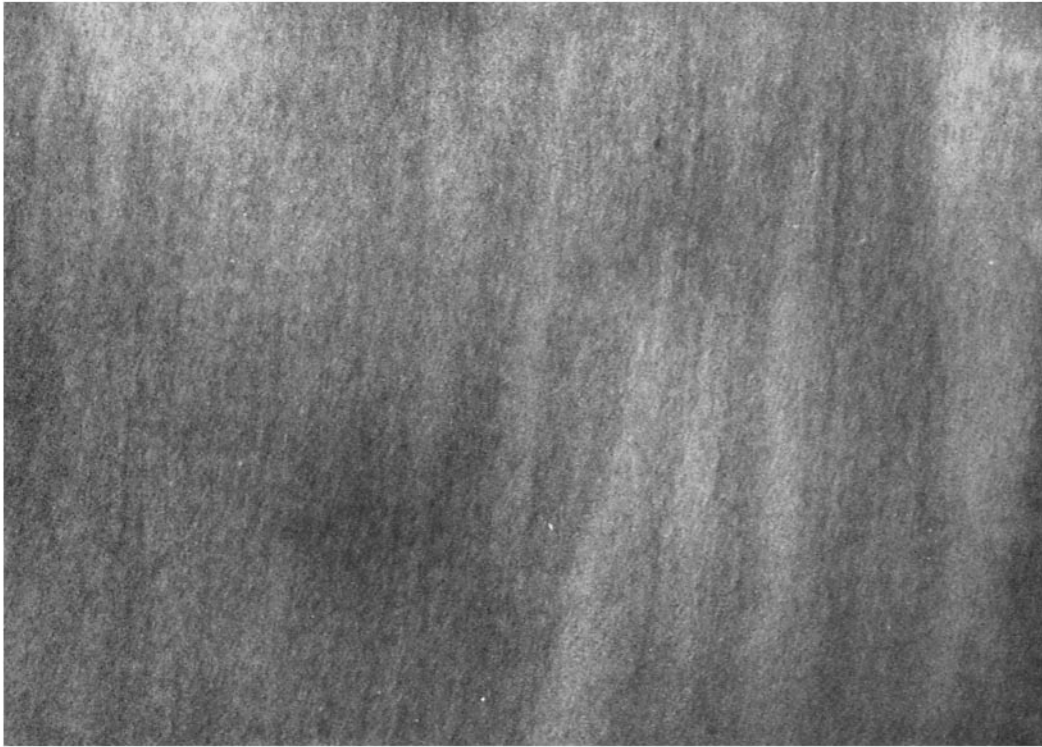FIGURE 45   A higher magnification of an unstained demineralized portion of the enamel matrix showing the arrangement of the parallel filaments in doublets and the 120 A spacing between the filaments comprising the doublet. Also note that some of the individual filaments comprising the doublet consist of two dense strands. The suggestion of axial periodic densities is also seen. Methacrylate. × 200,000.

REFERENCES

1. BEVELANDER, G., Calcification in molluscs. 3. Intake and deposition of Ca^{45} and P^{32} in relation to shell formation, *Biol. Bull.*, 1952, **102**, 9.
2. BEVELANDER, G., and BENZER, P., Calcification in marine molluscs, *Biol. Bull.*, 1948, **94**, 176.
3. DALTON, A. J., and ZEIGEL, R. F., A simplified method of staining thin sections of biological material with lead hydroxide for electron microscopy, *J. Biophysic. and Biochem. Cytol.*, 1960, **7**, 409.
4. DEAKINS, M., Changes in ash, water and organic content of pig enamel during calcification, *J. Dent. Research*, 1942, **21**, 429.
5. EASTOE, J. E., Organic matrix of tooth enamel, *Nature*, 1960, **187**, 411.
6. EASTOE, J. E., The amino acid composition of proteins from the oral tissues. II. The matrix proteins in dentin and enamel from developing human deciduous teeth, *Arch. Oral Biol.*, 1963, **8**, 633.
7. FEARNHEAD, R. W., Mineralization of rat enamel, *Nature*, 1960, **188**, 509.
8. FEARNHEAD, R. W., Electron microscopy of forming enamel, *Arch. Oral Biol.*, 1961, **4**, 24.
9. FEARNHEAD, R. W., and ELLIOTT, J. C., Observations on the relationship between the inorganic and organic phases in dental enamel, 5th International Congress for Electron Microscopy, Philadelphia, 1962 (S. S. Breese, Jr., editor), New York, Academic Press, Inc., 1962, **2**, QQ-7.
10. FRANK, R. M., SOGNNAES, R. F., and KERN, R., Calcification of dental tissues with special reference to enamel ultrastructure, *in* Calcification in Biological Systems, (R. F. Sognnaes, editor), Washington, American Association for the Advancement of Science, 1960, 163.
11. GLAS, J. E., Studies on the ultrastructure of dental enamel. 2. The orientation of the apatite crystallites as deduced from x-ray diffraction, *Arch. Oral Biol.*, 1962, **7**, 91.
12. GLAS, J. E., and OMNELL, K. A., Studies on the ultrastructure of dental enamel. 1. Size and shape of apatite crystallites as deduced from x-ray diffraction data, *J. Ultrastruct. Research*, 1960, **3**, 334.
13. GLIMCHER, M. J., Molecular biology of mineralized tissues with particular reference to bone, *Rev. Mod. Physics*, 1959, **31**, 359.
14. GLIMCHER, M. J., Specificity of the molecular structure of organic matrices in mineralization, *in* Calcification in Biological Systems, (R. F. Sognnaes, editor), Washington, American Association for the Advancement of Science, 1960, 421.

15. GLIMCHER, M. J., BONAR, L. C., and DANIEL, E. J., The molecular structure of the protein matrix of bovine dental enamel, *J. Mol. Biol.*, 1961, **3**, 541.
16. GLIMCHER, M. J., MECHANIC, G., BONAR, L. C., and DANIEL, E., The amino acid composition of the organic matrix of decalcified fetal bovine dental enamel, *J. Biol. Chem.*, 1961, **236**, 3210.
17. GLIMCHER, M. J., DANIEL, E., TRAVIS, D., and KAMHI, S., Electron optical studies of the organization of the inorganic crystals in embryonic bovine enamel, *J. Ultrastruct. Research*, in preparation.
18. GLIMCHER, M. J., FRIBERG, U., and LEVINE, P. T., The isolation and amino acid composition of the proteins of erupted bovine enamel, *Biochem. J.*, 1964, in press.
19. GLIMCHER, M. J., HODGE, A. J., and SCHMITT, F. O., Macromolecular aggregation states in relation to mineralization. The collagen hydroxyapatite system as studied *in vitro*, *Proc. Nat. Acad. Sc.*, 1957, **43**, 860.
20. GLIMCHER, M. J., MECHANIC, G. L., and FRIBERG, U., The amino acid composition of the organic matrix and the neutral and acid soluble components of embryonic bovine enamel, *Biochem. J.*, 1964, in press.
21. GLIMCHER, M. J., TRAVIS, D. F., FRIBERG, U., and MECHANIC, G., The electron microscopic localization of the neutral soluble proteins of embryonic bovine enamel, *J. Ultrastruct. Research*, 1964, in press.
22. GRÉGOIRE, C., DACHÂTEAU, G., and FLORKIN, M., La frame protidique des necres et des perles, *Ann. Inst. Oceanog., Paris*, 1955, **31**, 1.
23. JACKSON, S. F., The fine structure of developing bone in embryonic fowl, *Proc. Roy. Soc. London, Series B*, 1957, **146**, 270.
24. JOHANSEN, E., and PARKS, H. F., Electron microscopic observations on the three-dimensional morphology of apatite crystallites of human dentine and bone, *J. Biophysic. and Biochem. Cytol.*, 1960, **7**, 743.
25. KARNOVSKY, M. J., Simple methods for "staining with lead" at high pH in electron microscopy, *J. Biophysic. and Biochem. Cytol.*, 1961, **11**, 729.
26. LENZ, H., Elektronenmikroskopisch untersuchungen der schmelzgenese, *Deut. Zahnärztl. Z.*, 1958, **13**, 991.
27. LUFT, J. H., Improvements in epoxy resin embedding methods, *J. Biophysic. and Biochem. Cytol.*, 1961, **9**, 409.
28. MILLONIG, G., Advantages of a phosphate buffer for OsO$_4$ solutions in fixation, *J. Appl. Physics.*, 1961, **32**, 1637.
29. MILLONIG, G., A modified procedure for lead

staining of thin sections, *J. Biophysic. and Biochem. Cytol.*, 1961, 11, 736.

30. NEWMAN, W. F., and NEWMAN, M. W., The nature of the mineral phase of bone, *Chem. Rev.*, 1953, 53, 1.

31. NEWMAN, W. F., and NEWMAN, M. W., The Chemical Dynamics of the Bone Mineral, Chicago, The University of Chicago Press, 1958.

32. NYLEN, M. U., SCOTT, D. B., and MOSLEY, V. M., Mineralization of turkey leg tendon. 2. Collagen-mineral relations revealed by electron and x-ray microscopy, *in* Calcification in Biological Systems, (R. F. Sognnaes, editor), Washington, American Association for the Advancement of Science, 1960, 129.

33. NYLEN, M. U., and SCOTT, D. B., Electron microscopic studies of odontogenesis, *J. Indiana State Dent. Assn.*, 1960, 39, 406.

34. NYLEN, M. U., EANES, E. D., and ONNELL, K. A., Crystal growth in rat enamel, *J. Cell Biol.*, 1963, 18, 109.

35. PALADE, G. E., A study of fixation for electron microscopy, *J. Exp. Med.*, 1952, 95, 285.

36. PANNESE, E., Observations on the ultrastructure of the enamel organ. 1. Stellate reticulum and stratum intermedium, *J. Ultrastruct. Research*, 1960, 4, 372.

37. PANNESE, E., Observations on the ultrastructure of the enamel organ. 2. Involution of the stellate reticulum, *J. Ultrastruct. Research*, 1961, 5, 328.

38. PANNESE, E., Observations on the ultrastructure of the enamel organ. 3. Internal and external enamel epithelia, *J. Ultrastruct. Research*, 1962, 6, 186.

39. PIEZ, K. A., Amino acid composition of some calcified proteins, *Science*, 1961, 134, 841.

40. POOLE, D. F. G., and BROOKS, A. W., The arrangement of crystallites in enamel prisms, *Arch. Oral Biol.*, 1961, 5, 14.

41. REITH, E. J., The ultrastructure of ameloblasts from the growing end of rat incisors, *Arch. Oral Biol.*, 1960, 2, 253.

42. ROBINSON, R. A., An electron-microscopic study of the crystalline inorganic component of bone and its relationship to the organic matrix, *J. Bone and Joint Surg.*, 1952, 34, 389.

43. ROBINSON, R. A., and WATSON, M. L., Crystal-collagen relationships in bone as observed in the electron microscope. 3. Crystal and collagen morphology as a function of age, *Ann. New York Acad. Sc.*, 1955, 60, 596.

44. ROBINSON, R. A., and CAMERON, D. A., Electron microscopy of cartilage and bone matrix at the distal epiphyseal line of the femur in the new born infant, *J. Biophysic. and Biochem. Cytol.*, 1956, 2, 253.

45. RÖNNHOLM, E., An electron microscopic study of the amelogenesis in human teeth. 1. The fine structure of the ameloblasts, *J. Ultrastruct. Research*, 1962, 6, 229.

46. RÖNNHOLM, E., The amelogenesis of human teeth as revealed by electron microscopy. 2. The development of enamel crystallites, *J. Ultrastruct. Research*, 1962, 6, 249.

47. RÖNNHOLM, E., 3. The structure of the organic stroma of human enamel during amelogenesis, *J. Ultrastruct. Research*, 1962, 3, 368.

48. SCOTT, D. B., and NYLEN, M. U., Changing concepts in dental histology, *Ann. New York Acad. Sc.*, 1960, 85, 133.

49. SCOTT, D. B., and NYLEN, M. U., Organic-inorganic interrelationships in enamel and dentin: A possible key to the mechanism of caries, *Internat. Dent. J.*, 1962, 14, 417.

50. SOBEL, A. E., Local factors in the mechanism of calcification, *Ann. New York Acad. Sc.*, 1955, 60, 713.

51. STRATES, B., and NEWMAN, W. F., On the mechanism of calcification, *Proc. Soc. Exp. Biol. and Med.*, 1958, 97, 688.

52. THEWLIS, J., The structure of teeth as shown by x-ray examination, *Med. Research Council, Spec. Rep. Ser.*, 1940, 238.

53. TRAVIS, D. F., Matrix and mineral deposition in skeletal structures of the decapod crustacea, *in* Calcification in Biological Systems, (R. F. Sognnaes, editor), Washington, American Association for the Advancement of Sciences 1960, 57.

54. TRAVIS, D. F., The deposition of skeletal structures in crustacea. 1. The histology of the gastrolith skeletal tissue complex and the gastrolith in the crayfish, *Orconectes virilis* Hagen, *Biol. Bull.*, 1960, 118, 137.

55. TRAVIS, D. F., The deposition of skeletal structures in crustacea. 3. The histochemistry of the developing gastrolith and associated tissues in the crayfish, *Orconectes virilis* Hagen, *Acta Histochem.*, 1963, 15, 269.

56. TRAVIS, D. F., and FRIBERG, U., The deposition of skeletal structures in crustacea. 4. Micro-radiographic studies of the gastrolith of the crayfish, *Orconectes virilis* Hagen, *J. Ultrastruct. Research*, 1963, 8, 48.

57. TRAVIS, D. F., and FRIBERG, U., The deposition of skeletal structures in crustacea. 6. Micro-radiographic studies of the exoskeleton of the crayfish, *Orconectes virilis* Hagen, *J. Ultrastruct. Research*, 1963, 9, 285.

58. TRAVIS, D. F., Structural features of mineralization from tissue to macromolecular levels of organization in the decapod crustacea, *Ann. New York Acad. Sc.*, 1963, 109, 177.

59. TSUJI, T., SHARP, D. G., and WILBUR, K.,

Studies on shell formation. 7. The submicroscopic structure of the shell of the oyster, *Crassostrea virginica*, *J. Biophysic. and Biochem. Cytol.*, 1958, **4**, 275.

60. WADA, K., Crystal growth of molluscan shells, *Bull. Nat. Pearl Research Lab.*, 1961, **7**, 703.

61. WATABE, N., SHARP, D. G., and WILBUR, K. M., Studies on shell formation. 8. Electron microscopy of crystal growth of the nacreous layer of the oyster, *Crassostrea virginica*, *J. Biophysic. and Biochem. Cytol.*, 1958, **4**, 281.

62. WATABE, N., and WILBUR, K. M., Studies on shell formation. 9. An electron microscopic

study of crystal layer formation in the oyster, *J. Biophysic. and Biochem. Cytol.*, 1961, **9**, 761.

63. WATSON, M. L., Staining of tissue sections for electron microscopy with heavy metals. 2. Application of solutions containing lead and barium, *J. Biophysic. and Biochem. Cytol.*, 1958, **4**, 727.

64. WATSON, M. L., The extracellular nature of enamel in rats, *J. Biophysic. and Biochem. Cytol.*, 1960, **7**, 489.

65. WATSON, M. L., and AVERY, J. K., The development of the hamster lower incisor as observed by electron microscopy, *Am. J. Anat.*, 1954, **95**, 109.